Metal Oxide Nanocrystals and Their Properties for Application in Solar Cells

20

Ashish Dubey, Jiantao Zai, Xuefeng Qian, and Qiquan Qiao

Metal oxides have been of interest in processing, synthesis, characterization, and fabrication in both polymer-inorganic hybrid and dye-sensitized solar cells. TiO_2 [1–5], ZnO [6–9], CuO [10], and Nb_2O_5 [11] have been used as effective charge transport medium in solar cells. Different morphologies of these metal oxides have been synthesized for better charge transport across solar cells. These metal oxide nanostructures are chosen to provide large interfacial area and enhance charge transport across active layer. Metal oxide-based inorganic nanostructures can also improve environmental stability to cells, which is a major cause of degradation in cell performance. In this section, commonly used metal oxides (e.g., TiO_2, ZnO, Nb_2O_5, and CuO) will be discussed for their role in fabrication of polymer solar cells.

Processing and Synthesis of Metal Oxide Nanostructures

In the past decades, metal oxide nanostructures have attracted great interest due to their potential applications in optoelectronics. Controlling the size and shape of nanostructures is crucial in developing novel properties in nanoscience research. Considerable efforts have been devoted in obtaining various nanostructures such as nanoparticles, nanospheres, nanorings, nanopolyhedrons, nanorods, nanowires, nanobelts, and nanosheets [12, 13], which showed that nanostructure properties and device performance greatly depend on their size, morphology, composition,

Both Ashish Dubey and Jiantao Zai made equal contribution to this work.

A. Dubey • Q. Qiao (✉)
Department of Electrical Engineering and Computer Sciences, Center for Advanced Photovoltaics, DEH 219, South Dakota State University, Brookings, SD, USA
e-mail: ashish.dubey@sdstate.edu; qiquan.qiao@sdstate.edu

J. Zai • X. Qian
School of Chemistry and Chemical Engineering, State Key Laboratory of Metal Matrix Composites, Shanghai Jiao Tong University, Shanghai, China
e-mail: zaijiantao@sjtu.edu.cn; xfqian@sjtu.edu.cn

B. Bhushan et al. (eds.), *Handbook of Nanomaterials Properties*,
DOI 10.1007/978-3-642-31107-9_28,

and surface properties that can be tuned by synthetic methods. Numerous techniques have been developed to synthesize metal oxide nanostructures with a wide range of compositions, sizes, sophisticated crystallite shapes, and complex assembly properties. Although vapor-phase processing has been successfully employed for the preparation of metal oxide nanostructures, especially for one-dimensional nanostructures [14–17], solution-based chemical (wet chemistry) synthesis methods have become more versatile with regard to the controlled variation of structural, compositional, and morphological features. In fact, solution-based chemical synthesis such as sol–gel [18–22], chemical (co)precipitation [23], hydrothermal [24–28], combustion [29, 30], spray pyrolysis [31], microemulsion [25, 26, 32, 33–46], and electrospinning [24–28] has received considerable attention since they offer the possibilities to control homogeneity, purity of phase, size distribution, surface area, and microstructure uniformity. In this work, we will discuss general synthesis methods that are used to prepare several important semiconductors, such as TiO_2, ZnO, Nb_2O_5, CuO, and others with different nanostructures.

TiO_2

Historically, Fujishima and Honda reported electrochemical water splitting property on a TiO_2 electrode in 1972 [45, 47, 48], and Brian O'Regan introduced high surface area TiO_2 films in dye-sensitized solar cells in 1991 [49, 50]. TiO_2 is one of the most extensively studied materials with more than 80,000 publications over the past 5 years based on the database, web of knowledge. TiO_2, a large-band gap semiconductor, is known to be a very useful nontoxic, environmentally friendly, corrosion-resistant material used as pigment, paint, cosmetics, and catalyst. It has been widely studied with applications in photocatalysts, biosensors, and dye-sensitized solar cells (DSSCs) due to its unique optical and chemical properties [13, 34, 36, 47, 49, 51–55]. As a photocatalyst with large surface area, TiO_2 facilitates diffusion of photoinduced electrons and holes towards the surface before their recombination. TiO_2 having high dielectric constant and refractive index has also been widely used as optical coatings, beam splitters and antireflection coatings. In addition, TiO_2 has also been reported in use as humidity, hydrogen, and oxygen sensors [56–60]. TiO_2 has three crystalline polymorphs including anatase, rutile, and brookite. Rutile is a thermodynamically stable phase with smaller band gap than anatase. This section focuses on the recent progresses in the synthesis of TiO_2 nanostructures such as nanoparticles, nanorods, nanotubes, nanofibers, and various doping in TiO_2 nanostructures.

Nanoparticle

The anatase TiO_2 nanoparticles have been one of the most widely studied among various nanostructures with high surface area and strong absorption capacity. For industrial-scale production, the pyrolysis of $TiCl_4$ at high temperatures is used to produce Degussa P-25 TiO_2 nanoparticles. The laboratory scale synthetic approaches

to fabricate TiO_2 nanoparticles include sol–gel [61–65], hydrothermal [28, 63, 66], solvothermal [67, 68], chemical vapor deposition [16, 69, 70], and microemulsion [25, 26, 32]. Among them, hydrothermal is widely used for the production of small particles of TiO_2 [28, 63, 71–73]. TiO_2 nanoparticles can be synthesized by hydrothermal processing of either peptized precipitates of a titanium precursor with water [28] or titanium alkoxide in an acidic ethanol–water solution with particle sizes in the range of 7–25 nm by changing the concentration of Ti precursor and the solvents [63].

The sol–gel method from hydrolysis of a titanium precursor is another easy and widely used process to prepare TiO_2 nanoparticles. This process usually proceeds via a hydrolysis step of titanium alkoxide followed by condensation. A series of thorough studies have been conducted by Sugimoto et al. using the sol–gel method to prepare TiO_2 nanoparticles with different sizes and shapes by tuning the reaction parameters [74–78]. Under different pH conditions, the selective adsorption of shape controller on specific crystal planes of TiO_2 nanoparticles can tune the growth rate of these planes. Finally the size and shape is controlled by the growth rate in different crystal planes [74, 75]. Furthermore, the colloid dispersions of TiO_2 nanoparticles prepared by sol–gel method are efficient precursor to make various TiO_2 films on different substrates or nanostructures with various soft and hard templates [19, 21, 61, 73, 79–81].

Randomly Oriented and Highly Aligned Nanorods

TiO_2 nanorods can be used in novel photovoltaic devices including hybrid bulk heterojunction and dye-sensitized solar cells [82–84]. The synthesis of TiO_2 nanorods, especially arrays on the substrates, has attracted much attention. Weller et al. reported the controlled growth of high-aspect ratio anatase TiO_2 nanorods by hydrolysis of titanium tetraisopropoxide in oleic acid as surfactant at 80 °C [85]. Li et al. successfully synthesized the near monodisperse TiO_2 nanorods with their size, shape, and dispersibility controlled by adjusting reaction temperature, duration, and concentration of the reactants [68]. As previous mentioned, TiO_2 nanorods can be prepared by combining sol–gel method and anodic alumina membrane (AAM) template [34, 57]. TiO_2 nanorod arrays can be obtained by template-assisted sol–gel electrophoresis [18]. Direct oxidation of titanium metal plate with hydrogen peroxide can also produce crystalline TiO_2 nanorods [86]. For application in photovoltaic devices, developing a simple method to grow TiO_2 nanorod arrays on the transparent conductive substrates is important. The seed growth process is a commonly used method to prepare one-dimensional nanostructures on substrates. In order to prepare TiO_2 nanorod arrays, a TiO_2 polymeric sol prepared by sol–gel process was spin-coated on the fluorine-doped tin dioxide (FTO) substrate and then annealed as a seed layer, followed by the growth of nanorod arrays by hydrothermal method [42]. Aydil et al. invented a hydrothermal method for the first time to grow oriented, single-crystalline rutile TiO_2 nanorod films on FTO substrates (Fig. 20.1) by simply mixing hydrochloride with titanium precursors [87]. The acidity, concentration, additives of surfactants, processing temperature, and time were used to optimize the diameter, length, and density of the nanorods.

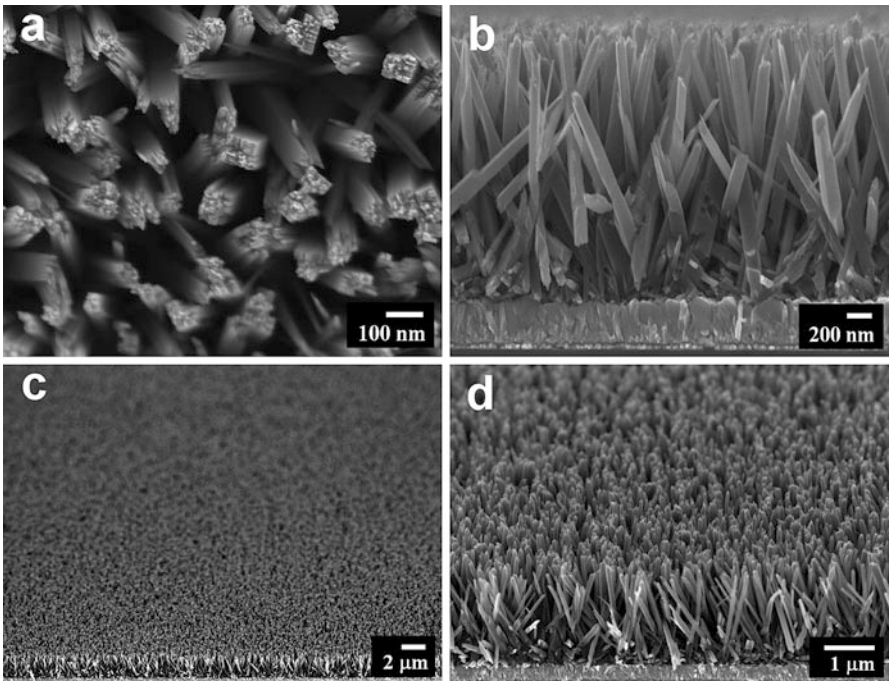

Fig. 20.1 FESEM images of oriented rutile TiO_2 nanorod film grown on FTO substrate in 30 mL of deionized water, 30 mL of hydrochloric acid, and 1 mL of titanium butoxide at 150 °C for 20 h. (**a**) Top view, (**b**) cross-sectional view, (**c**) and (**d**) tilted cross section (Reprinted (adapted) with permission from Ref. [87]. Copyright (2009) American Chemical Society.)

Nanotubes

The first titania nanotubes were probably synthesized by Hoyer through a template-assisted electrochemical deposition method in 1996 [88]. Since then, template-assisted methods [20, 89] and others including hydro-/solvothermal methods with or without templates [20, 24, 80, 90–92] and anodic oxidation method [89, 93, 94] have been reported. The hydrothermal method has been widely used to prepare TiO_2 nanotubes since Kasuga et al. reported that the hydrothermal treatment of TiO_2 particles in NaOH resulted in the formation of anatase TiO_2 nanotubes with large surface areas in 1998 [80]. Teng et al. further studied the structural features of nanotubes obtained by NaOH treatment on TiO_2 with different posttreatments [90]. Today, this method is widely used for preparing TiO_2 nanotubes. Crystallized TiO_2 nanotube arrays can be obtained by anodic oxidation of titanium foil and annealed at high temperature [43, 89, 93, 94]. The length and diameter of the TiO_2 nanotubes can be controlled over a wide range with an applied potential from 1 to 25 V in optimized phosphate/HF electrolytes. Depositing Ti film on the transparent conductive substrates, followed by an anodic oxidation process, has become a typical method to grow TiO_2 nanotube arrays [41, 44, 95, 96].

Nanofibers

TiO_2 nanofibers can be fabricated by the template-assisted sol–gel method with TiO_2 sol and porous alumina membranes or 'track-etched' polycarbonate filters as templates [20]. The template method is usually complex, cost- and time-consuming. Su et al. developed a soft hydrothermal chemical process via the reactions of amorphous TiO_2 gel (or commercial $TiOSO_4$ particles) and NaOH solution to synthesize TiO_2 nanofibers with high surface area [97]. Today, TiO_2 nanofibers can be conveniently prepared by electrospinning an alcohol solution that contains a polymer of high molecular weight and a titanium alkoxide precursor. Calcination in a subsequent step leads to the formation of polycrystalline nanofibers made of anatase TiO_2 with controllable diameters and interesting porous structures (Fig. 20.2) [56, 98–102]. Figure 20.2 shows extremely long TiO_2/polymer composite nanofibers (a) can be produced by electrospinning method, and the anatase TiO_2 nanofibers (b) with a diameter around 50 nm can be easily obtained by the calcination of these composite nanofibers.

Doping in TiO_2 Nanostructures

As a wide band gap semiconductor, TiO_2 can only utilize the ultraviolet light in solar spectrum. In order to extend its optical absorption to visible light region, doping metals or nonmetals into TiO_2 is well studied. Doping TiO_2 will mainly maintain TiO_2 crystal structure, but generate some favorable changes in their electronic and optical properties [12]. Typically, substitution of Ti^{4+} cations in TiO_2 with other transition metals is much easier than replacing O^{2-} anions with other anions due to the differences in charge states and ionic radii.

Three types of methods are typically used to dope TiO_2 nanostructures: wet chemistry, high-temperature treatment, and ion implantation on TiO_2 nanostructures. Wet chemistry usually realizes the doping by adding metal ion dopants to the titanium precursor, and then the mixed solution undergoes similar processes as the synthesis of pure TiO_2 nanostructures. Choi et al. successfully prepared TiO_2 nanoparticles doped with 21 different metal ions by sol–gel method and found the presence of metal ion dopants significantly influenced the photoreactivity, charge carrier recombination rates, and interfacial electron-transfer rates [103]. Nagaveni et al. performed a systematic study of W, V, Ce, Zr, Fe, and Cu ion-doped anatase TiO_2 nanoparticles by a solution combustion method and found that the solid solution formation was limited to a narrow range of concentrations of the dopant ions [30]. Li et al. synthesized highly crystalline and near monodisperse TiO_2 nanoparticles and nanorods doped by Sn, Fe, Co, and Ni ions by well-controlled solvothermal reactions [68]. Anpo et al. prepared TiO_2 nanoparticles doped with Cr and V ions with an ion implantation method. Plasma-enhanced CVD, ion beam-induced CVD, and radiation-frequency (RF) thermal plasma are also used to prepare metal-doped TiO_2 nanoparticles [12].

Some nonmetal elements such as B, C, N, F, S, Cl, and Br have also been successfully doped into TiO_2 nanostructures. Annealing the TiO_2 nanostructures under their corresponding gas flow is commonly used to synthesize nonmetal-doped TiO_2 nanostructures [12]. For example C- and F-doped TiO_2 nanomaterials can be

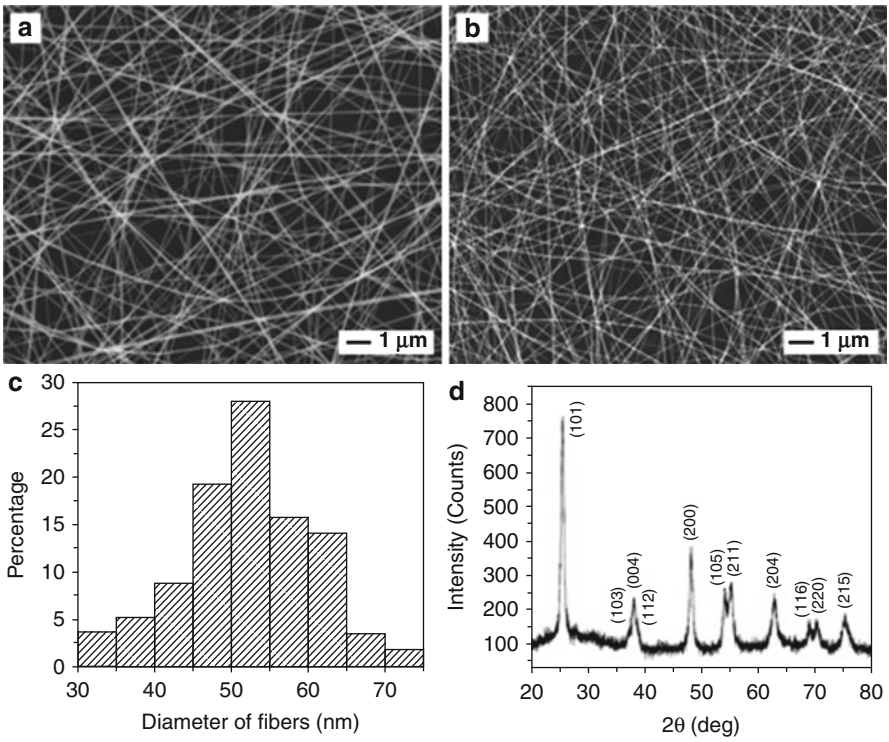

Fig. 20.2 (**a**) SEM image of TiO_2/PVP nanofibers that were electrospun from an ethanol solution containing $Ti(OiPr)_4$ (0.1 g/mL) and PVP (0.03 g/mL). The electric field strength was 1 kV/cm. (**b**) SEM image of the same sample after it had been calcined in air at 500 °C for 3 h. (**c**) Histogram showing the size distribution of nanofibers contained in the calcined sample. The size distribution was obtained from the SEM images of about 100 nanofibers. (**d**) XRD pattern of the same calcined sample. All diffraction peaks can be indexed to those of the anatase phase of titania (Reprinted (adapted) with permission from Ref. [101]. Copyright (2003) American Chemical Society.)

synthesized by heating TiO_2 under CO and hydrogen fluoride gas flow, respectively [104, 105]. Hydrolysis of titanium precursors in the solvent-containing dopants has also been reported. *N*-doped TiO_2 nanomaterials have been synthesized by the hydrolysis of titanium precursors in a water/amine mixture, followed by posttreatment of TiO_2 sol with amines [39, 106]. *S*-doped TiO_2 nanomaterials were synthesized by mixing TTIP with ethanol containing thiourea [107]. Cl^- and Br^- co-doped nanomaterials were synthesized by adding $TiCl_4$ to ethanol containing HBr [108].

ZnO

ZnO is a technologically important and environmental-friendly semiconductor with many remarkable properties, such as a direct wide band gap of 3.37 eV, large excitonic binding energy, high electron mobility, large piezoelectric constants, high

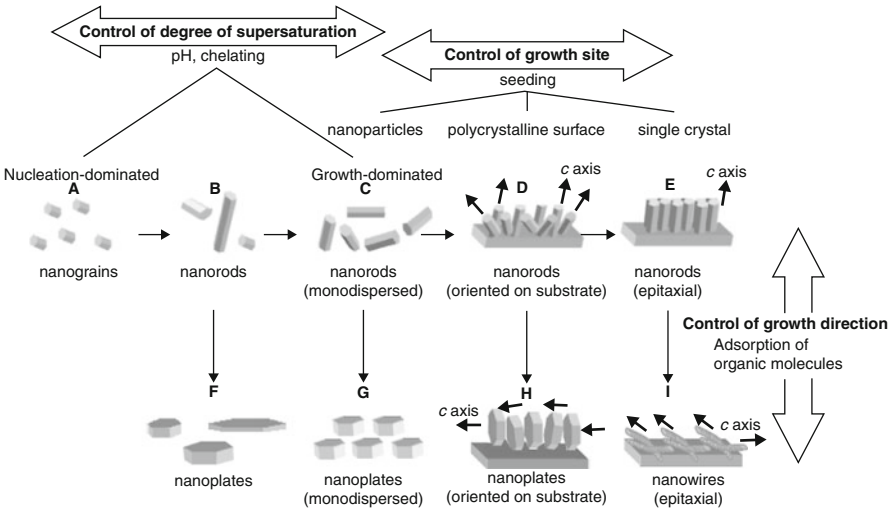

Fig. 20.3 Schematic illustration of the effects of the guiding parameters for the morphological design of ZnO crystals in solutions (Reproduced with permission from Ref. [119])

nonlinear optical coefficients, and radiation hardness. ZnO can be used in many applications including thin film transistors [109], sensors [110], solar cells [38, 111–115], UV photodetectors [116], and piezoelectric power generators [117, 118]. Because the ZnO properties determining the performance of ZnO-derived devices strongly depend on the size and shape, precise control of the morphology of ZnO nanostructures is of importance. Recently, wet chemistry attracted a lot of attention for its advantages such as low cost, low energy consumption, ease of large-scale production, and controllability of the morphology. And a wide variety of crystalline ZnO nanostructures and films were prepared using various solutions containing different chemicals, additives, and seeds or substrates by aqueous solution-based processing. Kawano [119] reviewed various morphologies of ZnO nanostructures and their dependence on preparation conditions including the source chemicals, the role of seeds or substrates, and the presence of organic molecules as a shape modifier. Figure 20.3 shows a schematic illustration of the effects of the guiding parameters. Under a high degree of supersaturation, fine grains are produced through a high rate of nucleation. On the other hand, nanorods elongated in the c direction can be obtained through gradual crystal growth with a low rate of the nucleation under a low degree of supersaturation. The presence of seeds could control the size distribution and crystal orientation. The ZnO nanostructures are basically controlled by tuning the growth rate, growth site, and growth direction. In addition, the degree of the supersaturation, the presence of seeds, and the adsorption of additives are other essential parameters. Many approaches including chemical vapor deposition [120], sputtering [121], sol–gel routes [31], and electrodeposition [46] have also been investigated as the size- and morphology-controlled synthesis method to prepare ZnO crystals.

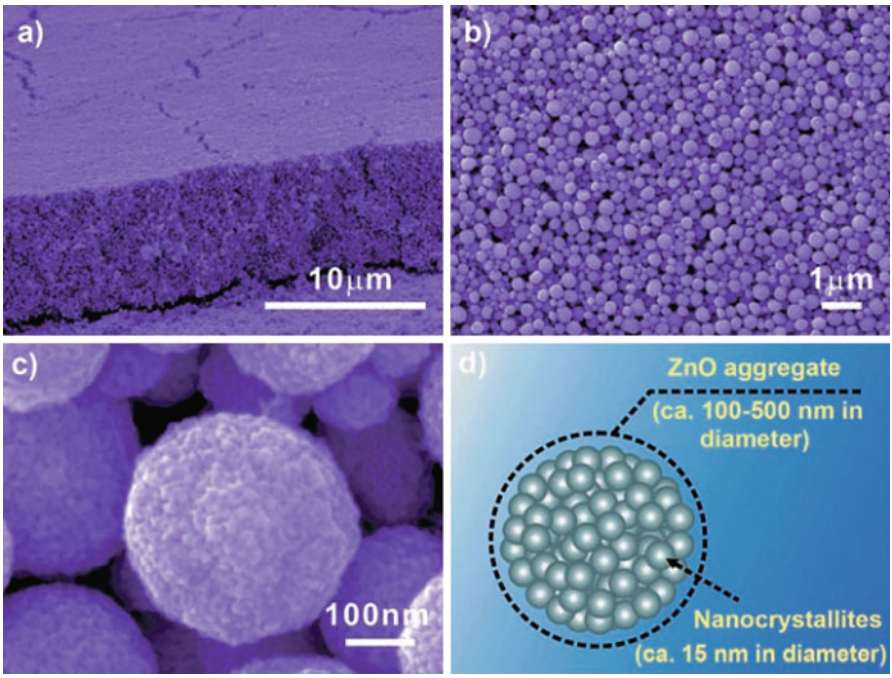

Fig. 20.4 Morphology and structure of the ZnO aggregate film: (**a**) SEM image of the cross section of the ZnO aggregate film, (**b**) SEM image of the top view of the ZnO film consisting of polydisperse aggregates, (**c**) magnified SEM image of an individual ZnO aggregate, and (**d**) schematic diagram illustrating the microstructure of aggregated ZnO comprising closely packed nanocrystallites (Reproduced with permission from Ref. [127])

Nanoparticles

Anderson et al. performed the synthesis of ZnO quantum dots (3–6 nm) by a sol–gel method with the addition of LiOH into an ethanolic zinc acetate solution [22]. They also studied the factors that influence the rate of particle growth [22]. Searson synthesized ZnO nanoparticles with different size by precipitation from solutions using $Zn(CH_3CO_2)_2$ and NaOH in a series of *n*-alkanols from ethanol to 1-hexanol [122]. ZnO nanoparticles were also been synthesized by ultrasonic irradiation of an aqueous-alcoholic/aqueous-alcoholic-ethylenediamine solution of zinc nitrate and sodium hydroxide [123]. Imai et al. prepared ZnO nanoparticles with size of 30–40 nm by dropping base solutions to Zinc salts solution under 60 °C [124]. Nanoparticles and superstructures of aggregated ZnO nanoparticles were also prepared by surfactant-assisted solvothermal method, where the anions and types of surfactants greatly affected the ZnO structures [125, 126]. Zhang et al. synthesized polydisperse ZnO aggregates by the hydrolysis of zinc precursor in polyol medium at 160 °C [127]. And then, a well-stacked ZnO porous film on FTO (Fig. 20.4) is fabricated by using

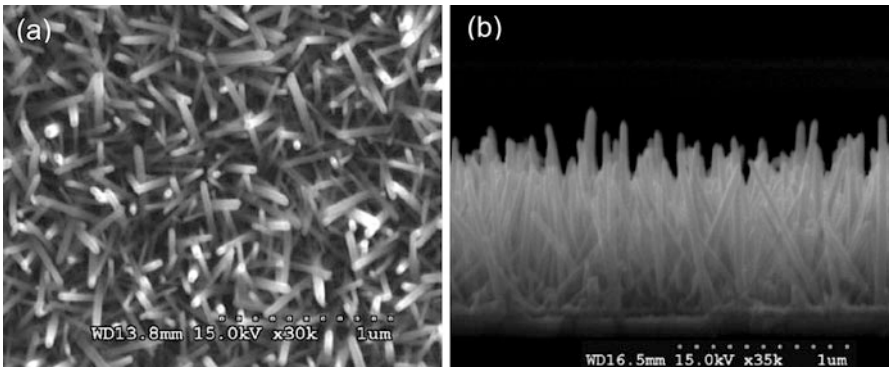

Fig. 20.5 (**a**) Top view and (**b**) cross-section SEM image of nd-ZnO (Reprinted (adapted) with permission from Ref. [114]. Copyright (2010) American Chemical Society.)

a drop-cast method. The film is assembled by spherical ZnO aggregates with different diameters, which consists of packed nanocrystallites. Spin coating of ZnO sol combined with calcinations is a common process to prepare thin film of ZnO nanoparticles on various substrates. Magnetron sputtering [121], pulsed laser deposition [17], and spray pyrolysis [128, 129] were also utilized to prepare ZnO nanoparticle films.

Randomly Oriented or Highly Aligned Nanorods

Chemical vapor deposition (CVD) is an efficient method to prepare ZnO nanorods on substrates. The partial oxygen pressure and chamber pressure are parameters that influence the growth mechanism and govern the final ZnO structure [130]. According to the epitaxial crystalline growth mechanism, ZnO nanorods can grow on (100) sapphire at a 30° angle to the substrate [131]. Lee et al. fabricated well-aligned, single-crystalline ZnO nanowires on GaAs substrates by metal-organic CVD [132]. Low-temperature growth routes on fused silica or Si substrates have also been reported [133]. Electrochemical deposition is another technique for achieving uniform and large area synthesis of ZnO nanostructures [46]. Growth of ZnO nanostructures can occur on a general substrate, flat or curved, without any seeds, as long as the substrate is conductive [37]. Under an external electric field, higher nanowire alignment and stronger adhesion to the substrate have been observed [37]. Vayssieres invented an aqueous method without template and surfactant to grow ZnO nanowires and oriented nanorod arrays [134]. Seed growth via a solution-based method is a typical process to prepare ZnO nanoarrays with different diameter, length, and density [114, 115, 135, 136]. ZnO nanocrystal seeds are coated onto cleaned fluorine-doped tin oxide (FTO) substrates firstly. And then the substrates that were immersed into a mixed solution of Zn-precursor, surfactant, and controlled-released bases underwent a chemical bath process to grow ZnO nanoarrays. And calcinations are usually used to improve the crystallinity of the products. Figure 20.5 shows the morphology of ZnO nanoarrays synthesized based on the

seed growth method by Yu et al. [114] The average diameter and length of the individual nanorods are ~ 40 nm and 1 μm, respectively.

Nanotower

Growth of ZnO nanocolumns on alumina substrates via oxidation of ZnS in a tube furnace at 950 °C has been reported [137]. The substrates were kept apart from the source at a lower temperature. The synthesized nanocolumns show a layered structure and become gradually thinner. This was attributed to be a result of a gradually decreasing supply of ZnO vapor. Qian et al. [138] developed a novel solution-based method to grow ZnO nanotower on the different substrates including glass, quartz, and polyethylene terephthalate (PET). The towerlike ZnO crystal arrays (Fig. 20.6a–c) were obtained in a reaction mixture solution containing zinc salt, ammonia, ammonium salt, and thiourea. The orientation of these tower like crystals could be controlled by the contents of these reactants at 95 °C. Other methods including CVD [139, 140], MOCVD [15], carbon thermal reduction method [141], and seed growth combined with hydrothermal processes have also been utilized to prepare ZnO nanotower.

Nanoflower

Qian et al. [138] also found that the flower-like ZnO arrays (Fig. 20.6d) can be obtained at 85 °C in the towerlike ZnO reaction solution system. Zhu et al. [142] synthesized flowerlike ZnO by a simple microwave-assisted solution phase approach using an ionic liquid (1-*n*-butyl-3-methyl imidazolium tetrafluoroborate). Gao et al. [143] performed flowerlike ZnO nanostructures on Si substrate from aqueous solution by the hexamethylenetetramine-assisted thermolysis of zinc-ethylenediamine complex at 95 °C for 1 h. Adschiri et al. [144] identified that a biomolecule, peptide, could recognize and generate ZnO nanoparticles to assemble into a highly ordered flower-type structure. Further researches indicate simply tuning the type and concentration of Zn-precursor/bases used in solution routes, ZnO flowers will be obtained [145–147]. In addition, hydrothermal [27, 148–150], eletrodeposition [33], and CVD methods [139, 151] are also used for the synthesis of ZnO nanoflowers.

Doping in ZnO Nanostructures

By controlling the doping level of ZnO, its electrical properties can be changed from insulator through n-type semiconductor to metal while maintaining optical transparency that makes it unique as a low-cost transparent electrode in flat-panel displays and solar cells to replace In-doped SnO_2 [31, 152, 153]. Mn-doped ZnO and Fe-, Co-, or Ni-alloyed ZnO were predicted to stabilize high-Curie-temperature ferromagnetism [154]. P-type doping in ZnO is also possible by substituting either group-I elements such as Li, Na, and K for Zn sites or group-V elements including N, P, and As for O sites [155]. Alloying ZnO with MgO (Eg = 7.7 eV) enables widening of band gap of ZnO and have been considered as a suitable material as barrier layers [156, 157]. However, when alloyed with CdO (Eg = 2.3 eV), it will narrow the band gaps to even the visible spectrum [158, 159]. The doping of ZnO films is usually utilized by CVD [158],

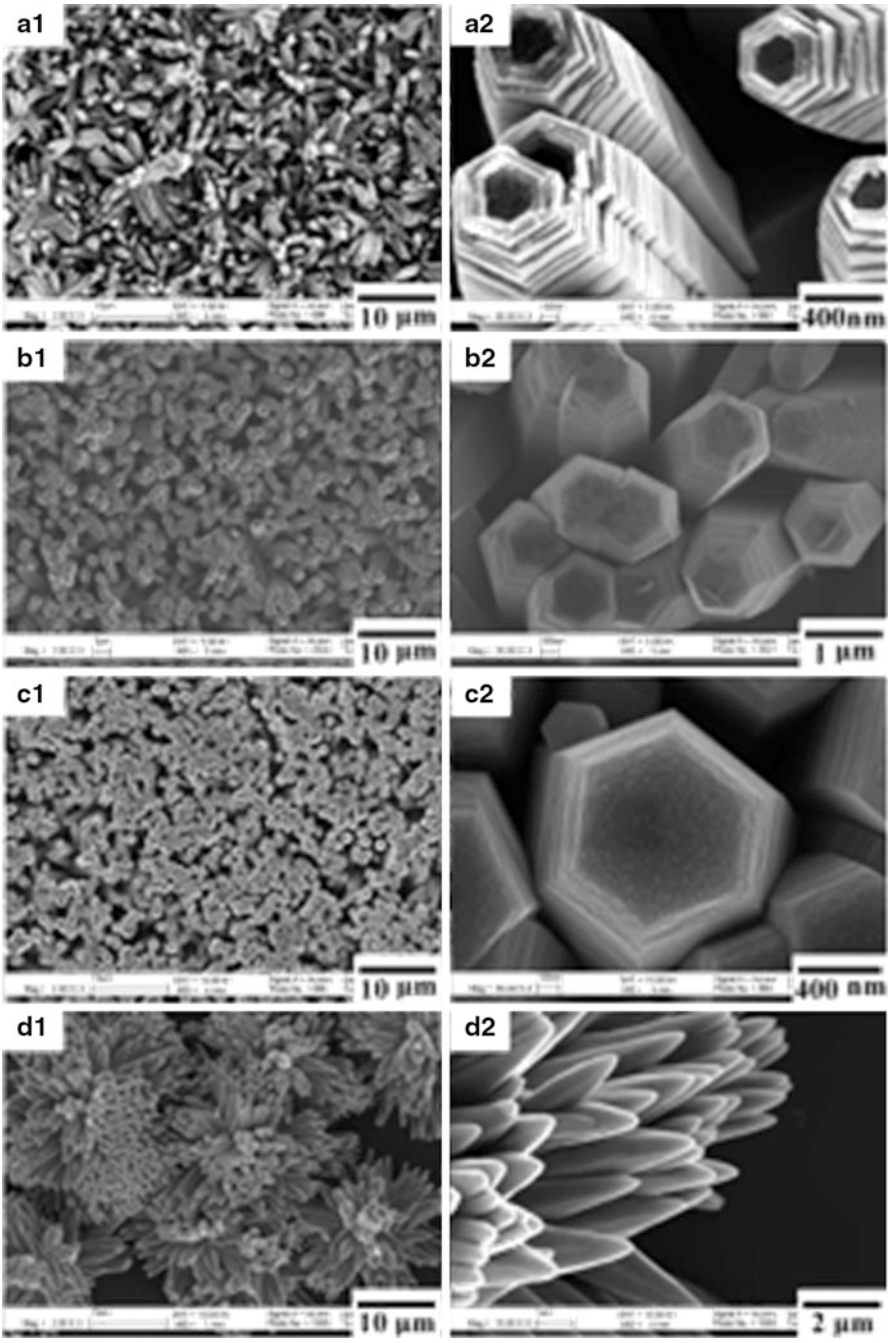

Fig. 20.6 (continued)

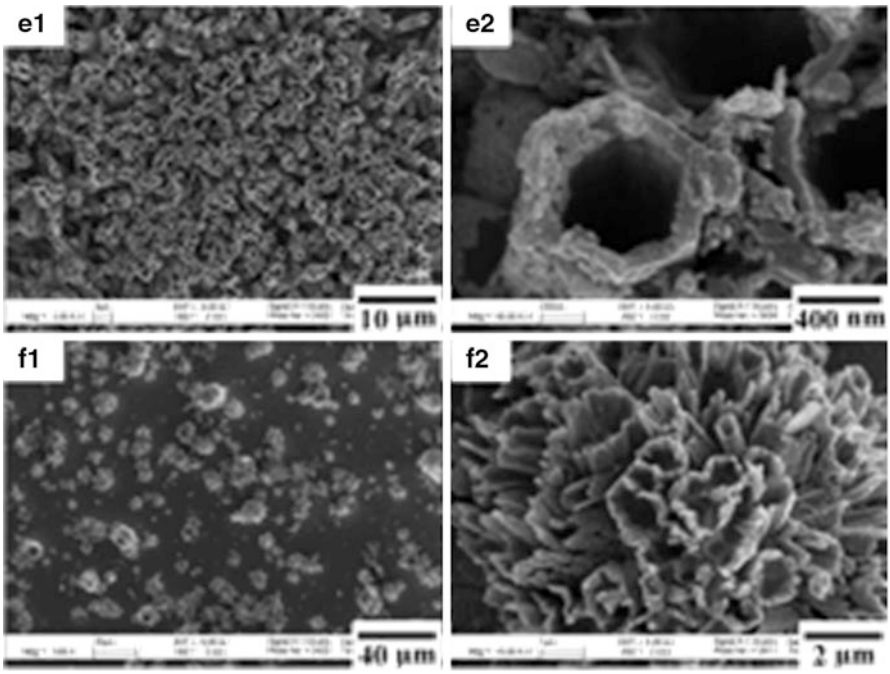

Fig. 20.6 FESEM images of the as-prepared towerlike, flowerlike, and tubelike ZnO arrays grown on glass substrate: (**a**–**c**) towerlike ZnO with general, better, and best orientation, (**d**) flowerlike ZnO, and (**e**, **f**) tubelike ZnO with high density and low density (Reprinted (adapted) with permission from Ref. [138]. Copyright (2004) American Chemical Society.)

MOCVD [14], molecular beam epitaxy [156], atomic layer deposition [160], and sputtering method [157]. Sol–gel process can be used to dope both ZnO film [31] and nanopowder [161]. The thermal decomposition of metal acetylacetonate precursors in a nonoxygen and nonpolar solvent is another method to prepare doped ZnO nanopowders, even the nanoink, a stable ZnO nanoparticle dispersion in the solvent [153].

Nb_2O_5 Nanoparticles

Nb_2O_5 is widely used in catalysts, gas sensors, electrochromic devices, and optical filters [162]. Up to now, several processes have been reported to synthesize Nb_2O_5 nanoparticles. Uekawa et al. prepared 4.5 nm sized Nb_2O_5 nanoparticles by heating the peroxoniobic acid sol obtained from the peptization of the acid precipitate with the H_2O_2 aqueous solution [163]. Zhou et al. prepared porous Nb_2O_5 nanoparticles via a solution-based method combined with calcination without the assistance of any surfactant [162]. Buha et al. synthesized Nb_2O_5 nanocrystals with size of 18–35 nm using a nonaqueous sol–gel route based on the solvothermal reaction

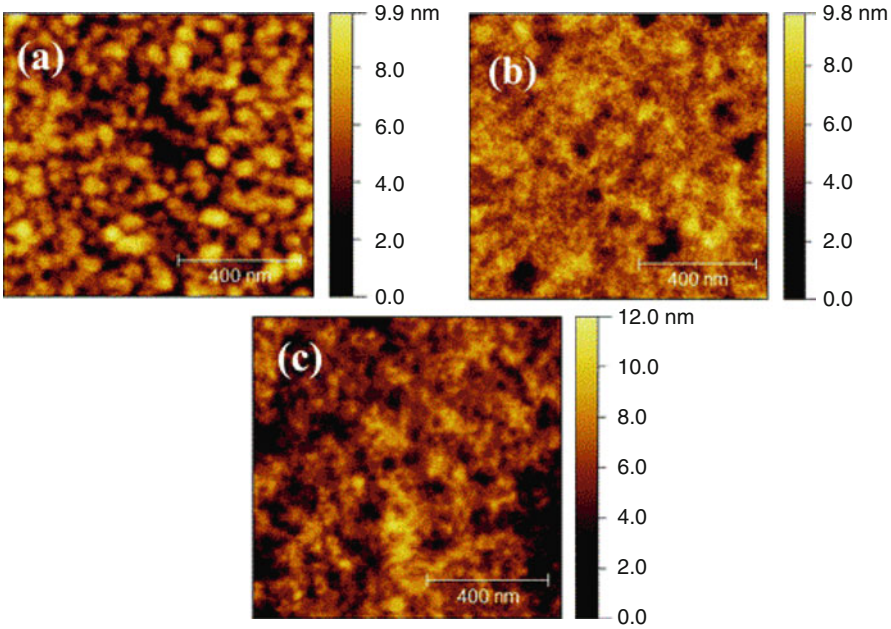

Fig. 20.7 Atomic force microscopy (AFM) topography image of (**a**) MDMO-PPV:PCBM active layer, (**b**) Nb_2O_5 ETL deposited on top of the MDMO-PPV:PCBM active layer, and (**c**) the pH neutral PEDOT:PSS HTL on top of the Nb_2O_5 layer (Reproduced with permission from Ref. [11])

of the corresponding metal chlorides with benzyl alcohol [164]. Recently, Qiao group grew Nb_2O_5 nanoparticles film by spin-coating the Nb_2O_5 sol–gel solution prepared by mixing the niobium ethoxide ($Nb(OC_2H_5)_5$) precursor with ethanol and acetic acid at room temperature and used the layer as a new electron transport layer for double junction polymer solar cells [11]. In particular, the preparation of Nb_2O_5 layer only takes half an hour and can be done at room temperature in an air atmosphere. When deposited by spin coating, the Nb_2O_5 sol–gel solution exhibited a high attachability on the polymer–fullerene active layer. Then the spin-coated film got oxidized quickly to form the Nb_2O_5 layer (Fig. 20.7).

CuO

As a p-type semiconductor, CuO exhibits a narrow band gap (1.2 eV) and shows wide applications in the field of emission materials, catalysts [165], gas sensors, magnetic storage media, electronics, and solar cells.

CuO Nanoparticles

Liu et al. prepared highly stable CuO nanoparticles with size of 2–4 nm in diameter (Fig. 20.8) by heating aqueous $Cu(CH_3COO)_2$ and urea solution in the presence of

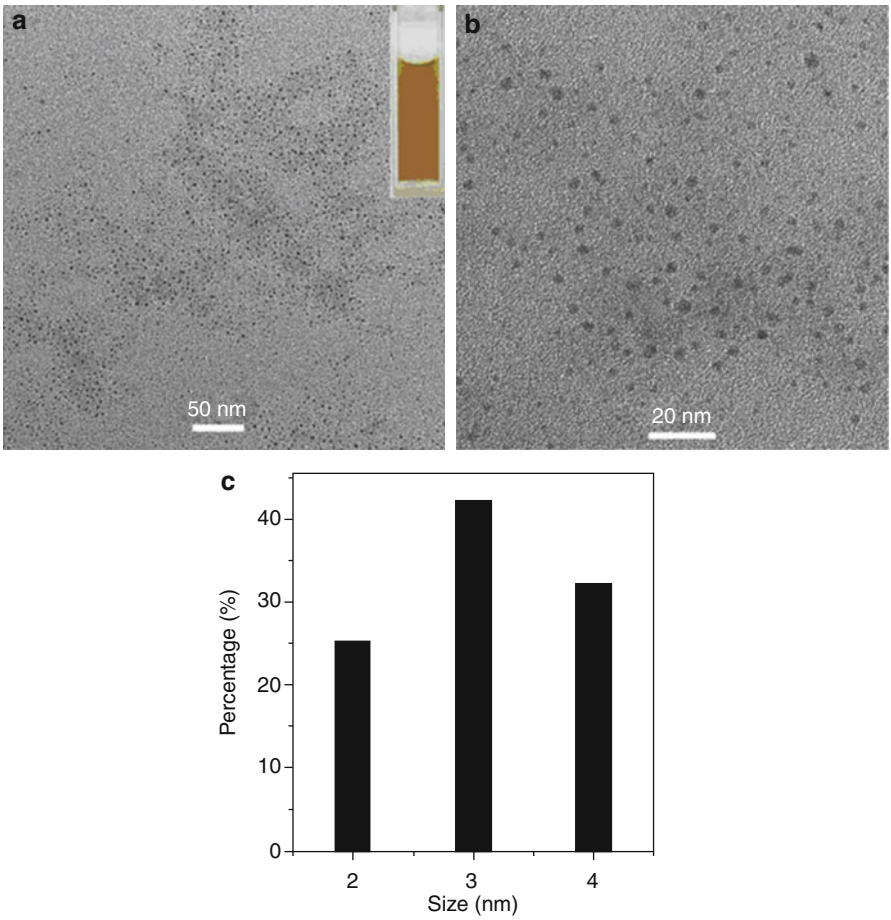

Fig. 20.8 (**a**) Low, (**b**) HRTEM images, and (**c**) their corresponding particle size distribution histogram of the products (inset: the photograph of CuO dispersion in water) (Reproduced with permission from Ref. [166])

poly[(2-ethyldimethylammonioethyl methacrylate ethyl sulfate)-co-(1-vinylpyrrolidone)] (PQ11) [166]. Wang et al. performed CuO nanoparticles with an average size of ca. 4 nm by microwave irradiation, using copper (II) acetate and sodium hydroxide as the starting materials and ethanol as the solvent [167]. Applerot et al. also reported a sonochemical method to synthesize CuO nanoparticles [168]. Solid-state synthesis [169], green synthesis via starch as surfactant [165], simple precipitation method [23, 170], and thermal decomposition [171] have also been used to prepare CuO nanoparticles.

CuO Hollow Spheres

Hollow nanostructures have been prepared to increase their surface area and reduce density for applications in drug delivery, chemical sensors, photonic devices, and

lightweight filler. A variety of methods have been developed to prepare nanostructures with hollow interiors [35, 172, 173]. Zeng et al. found that CuO hollow dandelion-like architectures by a one-pot hierarchical organizing scheme rely primarily on geometric constraints of building blocks [172]. Zhu et al. prepared a CuO hierarchical hollow nanostructure (Fig. 20.9), assembled by nanosheets, in *n*-octanol/aqueous liquid system through a microwave approach [174]. Controlled experiments revealed that both bubble and interface play key roles in determining the self-assembly process of CuO hierarchical hollow nanostructures. The morphology/size of building blocks and final products could be readily tuned by adjusting reaction parameters. Kong et al. synthesized CuO hollow nanospheres with an average diameter of 400 nm and shell thickness of 40 nm via a thermal oxidation strategy with Cu_2O solid nanospheres as the precursor [35]. The formation of CuO hollow nanospheres mainly result from the Kirkendall effect in the temperature-dependent experiments. Park et al. [175] synthesized uniform Cu_2O nanocubes by a one-pot polyol process, and the Cu_2O nanocubes were converted to polycrystalline CuO hollow nanostructures through a sequential dissolution–precipitation process, by adding aqueous ammonia solutions in air.

CuO Nanowires

Among various metal oxides, CuO has been extensively studied as a p-type metal oxide semiconductor [40, 176]. Jiang et al. described a vapor-phase approach to the facial synthesis of CuO nanowires supported on the surfaces of various copper substrates that include grids, foils, and wires [177]. Hansen et al. introduced and provided details on a large-scale, cost-effective pathway to fabricating ultrahigh dense CuO nanowire arrays by thermal oxidation of Cu substrates in oxygen ambient [178, 179]. The CuO nanowires that are produced by heating copper foil at 500 °C in a pure O_2 gas flow for 150 min feature an average length and diameter of ~15 μm and ~200 nm, respectively. Umar et al. demonstrated the preparation of a large-scale vertical array of single-crystalline CuO nanowires on different material surfaces [180]. The procedure simply involved a room-temperature liquid–solid growth process of attached CuO nanoseeds on ITO surface in the mixed aqueous solution of $Cu(CH_3COO)_2$ and NH_3. The field emission scanning electron microscopy (FESEM) image analysis indicated that these nanowires feature uniform size with tiny structures that have diameters and lengths in the range of 10 and 100 nm, respectively, and tend to form a bundle-like structure at the top end of the wires as shown in Fig. 20.10.

Applications of Metal Oxides in Solar Cells

Organic and organic/inorganic hybrid solar cells have attracted a lot of interest due to their solution-based processing and low cost [181–195]. Figure 20.11 shows the calculated 3D contour plots of polymer LUMO, polymer band gap, and

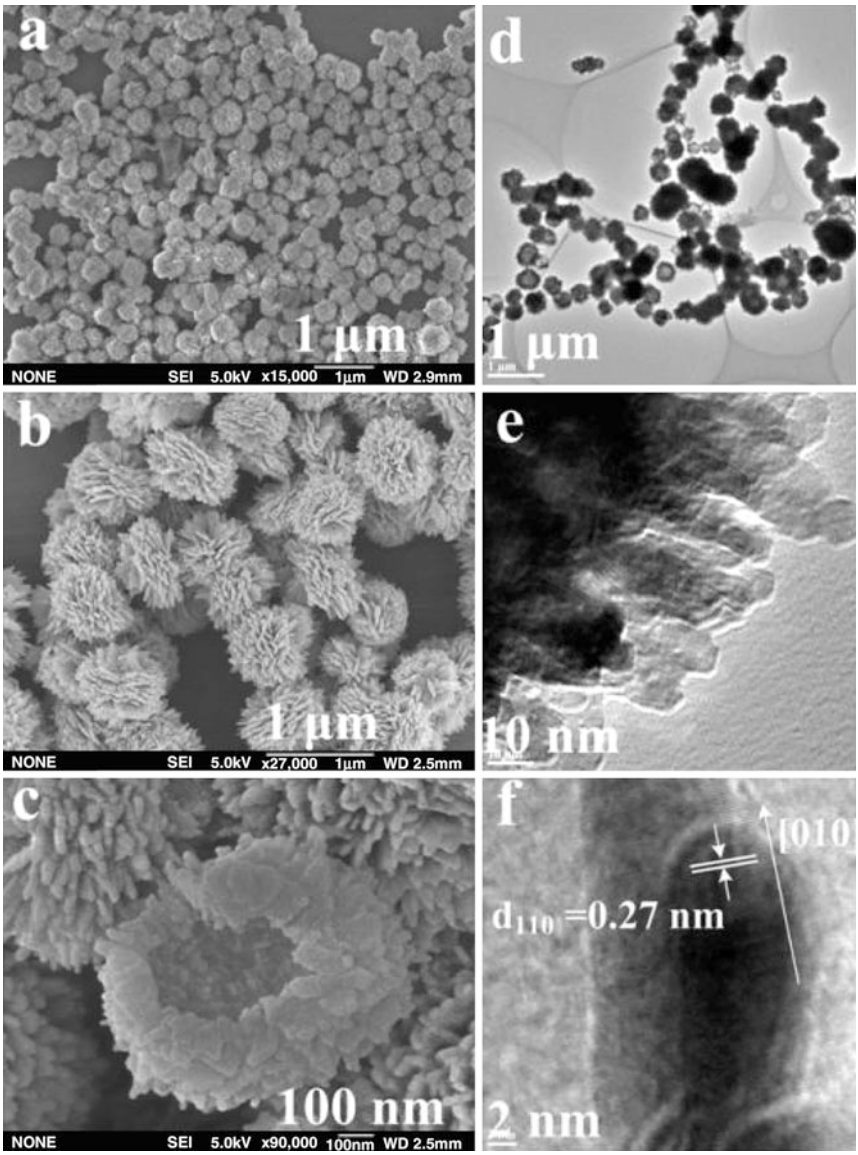

Fig. 20.9 SEM and TEM images of CuO obtained: (**a**) low-magnification SEM image, (**b**) enlarged SEM image, (**c**) FESEM image, (**d**) low-magnification TEM image, (**e**) enlarged TEM image, and (**f**) HRTEM image (Reprinted from Ref. [174], Copyright (2010), with permission from Elsevier.)

cell efficiency with three typical inorganic acceptors of (a) TiO_2, (b) ZnO, and (c) CdSe. It can be seen that the polymer band gaps are almost the same at ~1.5 eV; however, their LUMO and HOMO energy levels are different depending on what acceptor materials will be used [188].

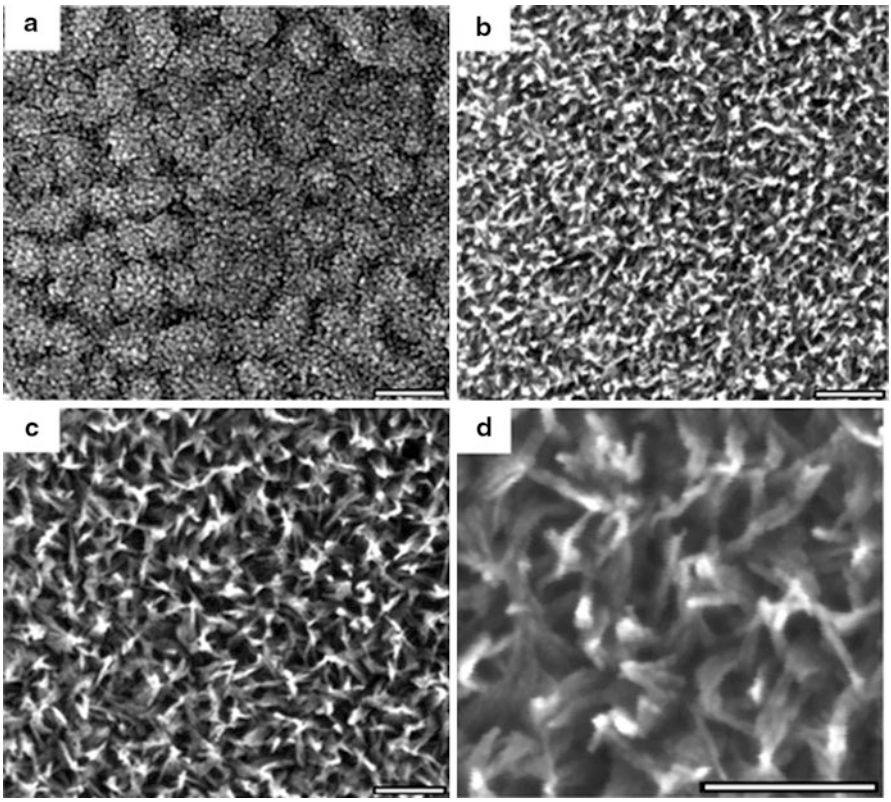

Fig. 20.10 (**a**) FESEM image of CuO nanoseed particles prepared using an alcohothermal method for 2 h at 250 °C; (**b**, **c**) FESEM images of CuO NWs grown at different growth periods in the mixed aqueous solution of 10 mM $Cu(CH_3COO)_2$ and 12 mM NH_3 for (**b**) 2 and (**c**) 15 h at room temperature (25 °C); (**d**) high-magnification image of (**c**). Scale bars are 100 nm (Reprinted (adapted) with permission from Ref. [180]. Copyright (2007) American Chemical Society.)

Titanium Dioxide (TiO_2)

Different nanostructures (e.g., nanoparticles, nanotubes, and nanofibers) of TiO_2 have been employed for fabricating efficient solar cells. Kwong et al. in 2003 reported the use of TiO_2 nanoparticle with poly(3-hexylthiophene) (P3HT) to make a nanocomposite film acting as an active layer [196]. Photoluminescence spectrum of active layer films showed quenching of P3HT emission for all different concentrations of TiO_2 which was mixed with P3HT. Cells made from 50 % and 60 % TiO_2 concentrations showed improved performance than those made with TiO_2 concentrations as 40 % (lowest) and 70 % (highest). Poor performance for lower concentration (40 %) of TiO_2 was attributed to recombination of dissociated charges, whereas higher concentration (70 %) of TiO_2 led to poor film quality. Solvent selection for mixing

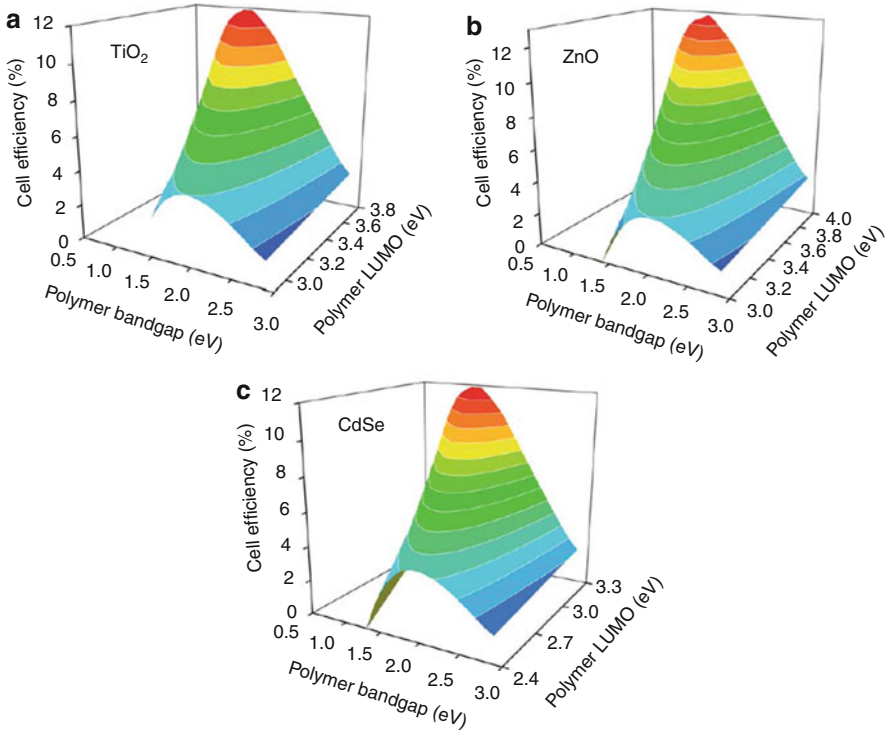

Fig. 20.11 Calculated relationship between polymer band gap (E_g), polymer LUMO, and cell efficiency in single junction hybrid solar cells with three representative inorganic acceptors of (a) TiO_2, (b) ZnO, and (c) CdSe. The efficiency was calculated with IPCE = 65 %, FF = 60 % under AM 1.5 with an incident light intensity of 100 mW cm^{-2}. (Reproduced from Ref. [188] with permission from The Royal Society of Chemistry)

TiO_2 and P3HT also affected the performance of fabricated cell. Cell fabricated with 60 % TiO_2, using xylene as solvent gave best performance. Qiao et al. also used TiO_2 nanoparticles to blend with a water soluble polymer (PTEBS) and demonstrated potential to develop environmentally friendly solar cells [82, 197–199]. Yang et al. studied the effect of adding TiO_2 nanotubes into P3HT:PCBM blend on device performance in 2010 [200]. Conventional device structure was fabricated with device structure as glass/ITO/PEDOT:PSS/P3HT:PCBM:TiO_2/LiF/Al (Fig. 20.12a). Active layer films were prepared by adding TiO_2 nanotubes in P3HT:PCBM solution, followed by sonication for 30 min, in order to disperse it uniformly. The solution was then stirred and spin-coated on top of PEDOT:PSS, followed by thermal deposition of LiF (1 nm) and Al (100 nm). Finally the device fabricated was annealed at 150 °C for different time period to optimize morphology of active layer.

From Fig. 20.12b, it was observed that TiO_2 nanotube aggregates are made from many individual nanotube each having diameter of ~10 nm. The TiO_2 aggregates as a whole had diameter of 300–600 nm, which was much larger than the films

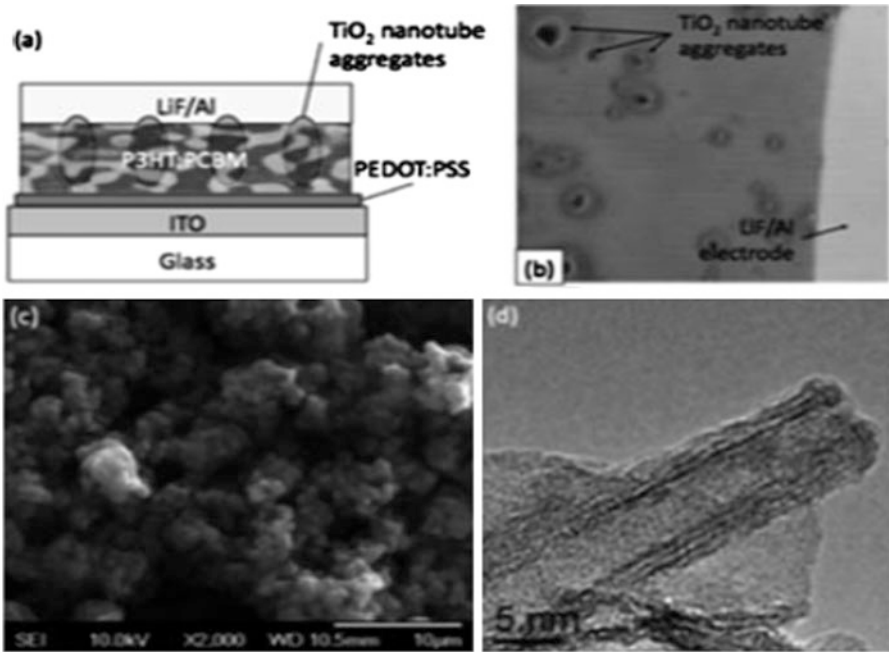

Fig. 20.12 (**a**) Device structure of TiO_2 nanotube-based solar cells, (**b**) optical image of fabricated solar cell surface taken at × 500, (**c**) SEM micrograph of TiO_2 nanotubes, and (**d**) TEM micrograph of TiO_2 nanotubes (Reproduced from Ref. [200] with permission from The Royal Society of Chemistry)

made from P3HT:PCBM (140 nm). The surface roughness of active layer film therefore increased after adding TiO_2 nanotube aggregates. J-V curves of the control sample without TiO_2 aggregates annealed for 9 min showed an efficiency of 2.8 %, whereas device with TiO_2 aggregates annealed for 5 min showed an efficiency of 3 % with an open circuit voltage (V_{oc}) of 0.68 V, short circuit current (J_{sc}) of 0.60, and power conversion efficiency (PCE) of 3.2 %.

Liao et al. reported hybrid solar cells made from nanostructured arrays of TiO_2/P3HT in 2012 [201]. The hybrid cell was modified by introducing Z907 and D149 dye molecule showing enhancement in device performance. Introduction of dye molecules enhanced light absorption and improved the TiO_2 nanostructure/P3HT interface. Dye molecule acted as a bridge to link TiO_2 and P3HT, where the dye carboxylic group links with hydrophilic TiO_2 and the dye aryl group connects with hydrophobic P3HT. Rutile TiO_2 nanorod (NR) nanoarrays and nanodendrite (ND) structure were used with P3HT to fabricate hybrid solar cells. TiO_2 NR and ND structures were modified by treating it with $TiCl_4$ to form nanoparticles on NR and ND surface, thus increasing the surface area. Figure 20.13 shows top and cross-sectional SEM micrograph of TiO_2 nanorods treated with $TiCl_4$. TiO_2 NR and ND structure act as electron acceptor and provide transport pathway in TiO_2/P3HT-based hybrid cell. Two types of device were fabricated: one without any dye modification and the other with dye attached onto both TiO_2 NR and TiO_2 ND.

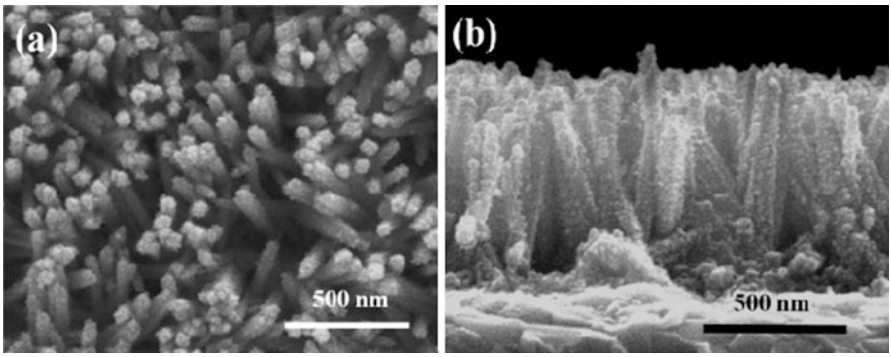

Fig. 20.13 (**a**) Top view and (**b**) cross-sectional TiO_2 nanorod SEM images of $TiCl_4$ treated TiO_2 NR (Reprinted (adapted) with permission from Ref. [201]. Copyright (2012) American Chemical Society.)

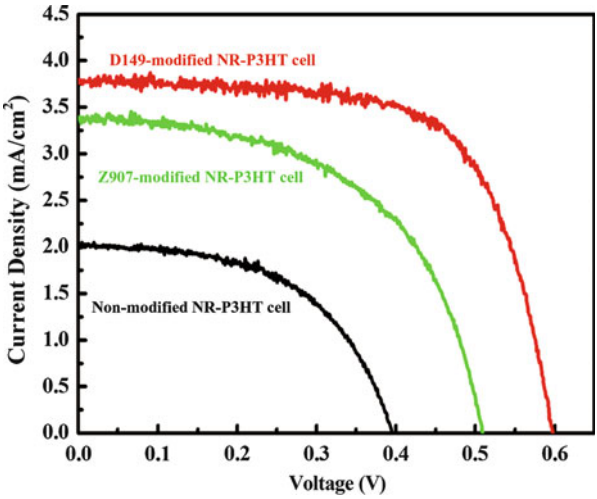

Fig. 20.14 J-V plot for non-modified, Z907 dye modified, D149 dye modified TiO_2 NR array-/P3HT-based hybrid cell (Reprinted (adapted) with permission from Ref. [201]. Copyright (2012) American Chemical Society.)

J-V characteristics of non-modified TiO_2 NR/P3HT solar cells showed poor device performance with efficiency of 0.43 %. The Z907 and D149 dye modified cells exhibited higher efficiency at 0.94 % for Z907 and 1.58 % for D149. The devices were made by using 650 nm thick TiO_2 nanorod arrays. Figure 20.14 shows device performance without and with dyes attached onto TiO_2 as surface modifier.

Further enhancement in solar cell performance was observed by using 1.5 μm thick TiO_2 NR array and 1.5 μm thick ND array with D149 dye modification. J-V curves showed a significant performance improvement with increasing thickness of TiO_2 nanostructured array with TiO_2 ND (1.5 μm)–P3HT-based cell showing highest power conversion efficiency at 3.12 % (Fig. 20.15).

Xu et al. in 2012 studied charge transfer in P3HT–TiO_2 nanorod composite by photoluminescence quenching [83]. Three different samples were prepared: In first

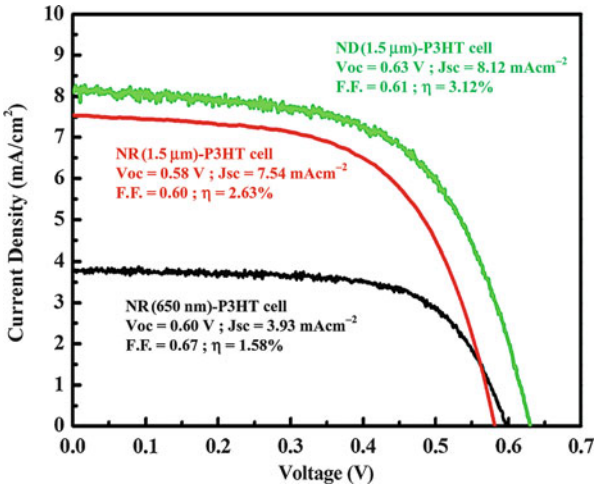

Fig. 20.15 J-V plots of TiO_2 NR array (650 nm thick)/ P3HT modified with D149 dye molecules, D149 modified TiO_2 NR array (1.5 μm thick)/P3HT, and D149 modified TiO_2 ND array (1.5 μm thick)/P3HT (Reprinted (adapted) with permission from Ref. [201]. Copyright (2012) American Chemical Society.)

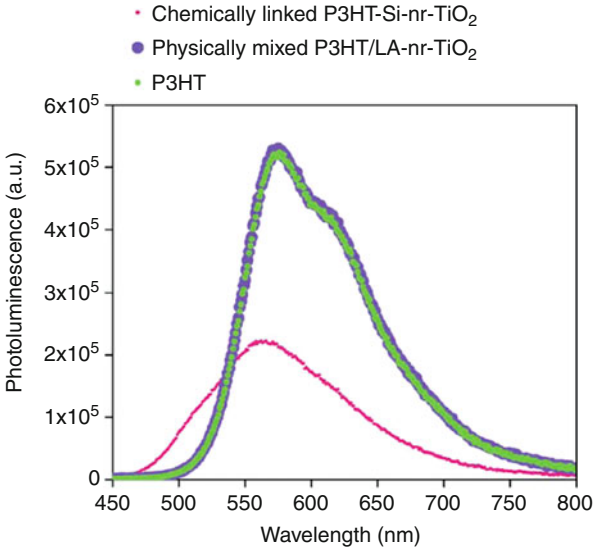

Fig. 20.16 Photoluminescence spectra of chemically linked P3HT–Si–nr–TiO_2, physically mixed P3HT/LA–nr–TiO_2, and pristine P3HT. The measurement was taken at excitation wavelength of 420 nm (Reproduced from Ref. [83] with permission from The Royal Society of Chemistry)

sample P3HT was chemically linked with TiO_2 nanorod (nr) by a linker triethoxy-2-thienylsilane (P3HT–Si–nr–TiO_2), second sample was composite of P3HT and TiO_2 (P3HT/LA–nr–TiO_2), made by physical mixing of P3HT and linoleic acid (LA) capped TiO_2 nanorods, and third sample was pristine P3HT itself. Steady state photoluminescence quenching spectra of all three samples were recorded (Fig. 20.16). Photoluminescence quenching was observed in P3HT chemically

linked with TiO_2 nanorods, which was attributed to charge transfer occurring between P3HT and TiO_2 nanorods, whereas physically mixed P3HT–TiO_2 nanorods showed overlap of PL spectrum with pristine P3HT spectrum, indicating no charge transfer occurring in P3HT–TiO_2 composite.

ZnO

ZnO, an n-type material, is used as electron acceptor along with electron-donating polymer in fabricating organic–inorganic hybrid solar cell. ZnO acts as electron transport layer with good electron mobility and is solution processable and environmentally stable. Beek et al. in 2006 reported hybrid solar cells made from blend of ZnO nanoparticles and P3HT with efficiency ~ 0.9 % [7]. Hau et al. in 2008 reported inverted polymer solar cell utilizing ZnO as electron transport layer [202]. Charge collection in inverted solar cell is reverse of regular device structure, in which electrons are collected at front electrode, and holes are collected at back metal electrode. Regular device with structure of ITO/PEDOT:PSS/P3HT:PCBM/LiF/Al and inverted cell with structure of ITO/ZnO/P3HT:PCBM/PEDOT:PSS/Ag were fabricated and tested. Inverted P3HT:PCBM blend (1:0.6 by weight) with a film thickness of 200 nm achieved an efficiency of $\sim$3.5 %. Regular device structure gave an efficiency of $\sim$2.4 %. Fill factor for both device structures was comparable, but J_{sc} and V_{oc} were higher in inverted devices, partly attributed to high interfacial area provided by ZnO nanoparticle layer.

Stability studies of conventional and inverted device were carried out by keeping them in ambient condition and measuring their performance for 40 days. In regular device, it was observed that cell efficiency reduced to less than half of its original value in 1 day and got totally degraded after 4 days (Fig. 20.17a). On the other hand, inverted device was found to be highly stable for 40 days (Fig. 20.17b). All the device parameters remained comparable except J_{sc}, which slightly decreased. In inverted cells, silver electrode can form silver oxide layer in air and thus increase its work function to -5.0 eV. The work function then matches better with HOMO of PEDOT:PSS that is -5.1 eV. Inset of Fig. 20.17a shows the diode behavior in dark condition. The current density at 2 V on the J-V curves of fresh regular solar cells is 2 orders higher that of solar cells left in air for 4 days. However, inverted device shows a much higher stability with V_{oc} and FF remaining almost the same, while J_{sc} decreases slightly. Their dark condition J-V curves are also comparable as shown in inset of Fig. 20.17b.

In 2013, Ka et al. studied the ZnO annealing effects on performance of inverted solar cells [203]. Devices fabricated with ZnO annealed at a low temperature of 80 °C exhibited an efficiency of 3.6 % that is comparable to devices processed at higher annealing temperatures. Several characterization results concluded that the optimum efficiency at low temperature annealing was attributed to improvement in band energy alignment, crystallinity, and relative ZnO amount. Device structures and their J-V curves under different ZnO annealing temperatures are shown in

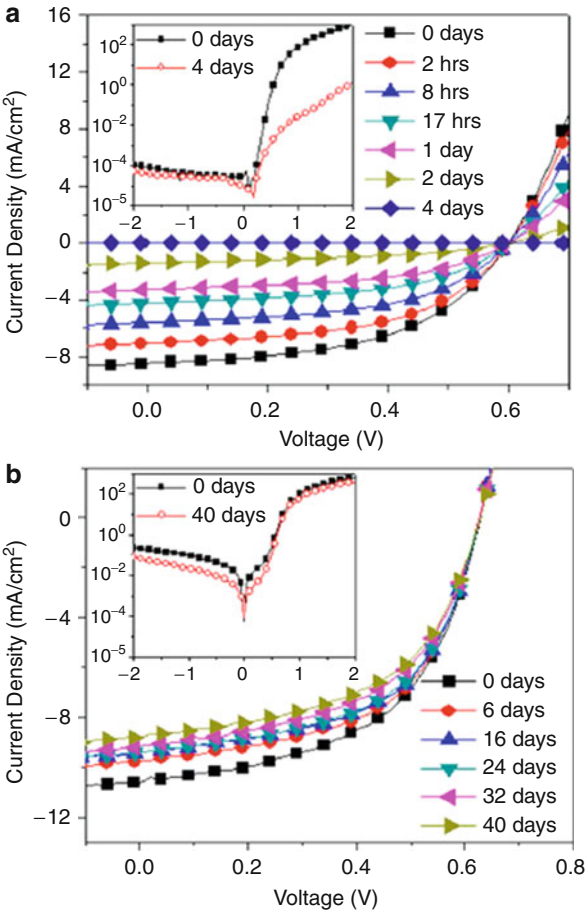

Fig. 20.17 J-V plots of (**a**) regular solar cells characterized in ambient condition over a period of 4 days and (**b**) inverted solar cell tested in ambient condition over a period of 40 days (Reprinted with permission from Ref. [202]. Copyright (2008) AIP Publishing LLC.)

Fig. 20.18. For devices with annealing temperatures (T_a) at 25 °C and 60 °C, J-V curve shows S-shape in nature, indicating inefficient and/or unbalanced electron and hole transport to electrodes, therefore leading to cell efficiency (η) lower than 0.2 %. When the annealing temperature increased to 70 °C, the J-V characteristics improve a lot, leading to a J_{sc} of 9.7 mA/cm^2, V_{oc} of 0.59 V, FF of 0.49, and η of 2.6 %. When further increased to 80 °C or above, device efficiency increased to 3.61 % with a higher fill factor at 0.61. Further increase in ZnO annealing temperature (T_a) to 90 °C and 150 °C resulted in similar device performance as observed for $T_a = 80$ °C (Fig. 20.18).

Xu et al. in 2013 fabricated organic–inorganic hybrid solar cells and studied donor–acceptor interface by Kelvin probe force microscopy [189]. Cell structure consisted of ITO/ZnO/P3HT/Ag, where two different structures of ZnO (nanoridges and nanorods) were used as active layer for fabricating two different

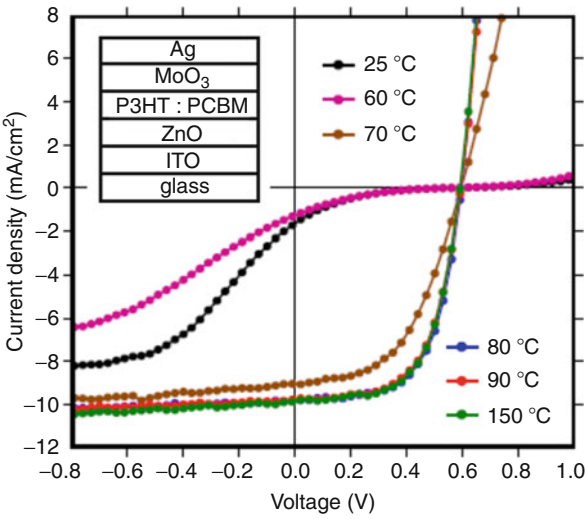

Fig. 20.18 J-V plots of inverted polymer solar cells with ZnO as electron-selective layer, treated at different annealing temperatures. Device structure of inverted polymer solar cells is also shown in inset (Reprinted from Ref. [203]. Copyright (2013), with permission from Elsevier.)

cells. P3HT was spin casted on ZnO films, followed by annealing at 150 °C, for 10 min. Topography and interface studies of ZnO/P3HT films were studied by atomic force microscope (AFM) and Kelvin probe force microscopy (KPFM). Topography of ZnO nanoridge films showed wrinkled shaped morphology which was attributed to stress relaxation caused by slow drying process of film (Fig. 20.19). Surface potential (SP) across the interface of P3HT/ZnO was studied by KPFM, which showed higher SP value for P3HT and lower SP value for ZnO nanoridge region (Fig. 20.19). Surface potential of the interface was measured under dark and illuminated condition. A 0.1 V difference in SP was seen under dark condition and 0.25 V difference under illuminated condition and was attributed to light response of P3HT and ZnO (Fig. 20.19). P3HT shows better light response in comparison to ZnO; therefore, P3HT exhibited higher surface potential than ZnO, allowing a favorable path for electron transfer to ZnO.

Nb_2O_5

Nb_2O_5 is new in the list of oxides, towards which researchers have been showing interest to use as electron transport layer for solar cells. In 2011, Wiranwetchayan et al. reported the use of Nb_2O_5 in fabricating inverted solar cells [204]. A thin film of Nb_2O_5 was introduced in between fluorine-doped tin oxide (FTO) and active layer (P3HT:PCBM) with device structure as glass/FTO/Nb_2O_5/P3HT:PCBM/PEDOT/Ag. The sol of Nb_2O_5 was used for spin coating a thin film of Nb_2O_5 on FTO, followed by annealing at 450 °C for 1 h to make it crystalline.

Photovoltaic response of the devices without and with Nb_2O_5 was studied. The devices without Nb_2O_5 showed no photovoltaic response; however, devices having a thin film of Nb_2O_5 exhibited an efficiency of 2.7 %. Dependence of film thickness on device efficiency was also studied. The efficiency decreased to zero with increasing thickness. This was attributed to the Nb_2O_5 film thickness increasing more than tunneling path length. As conduction band of Nb_2O_5 is higher than the

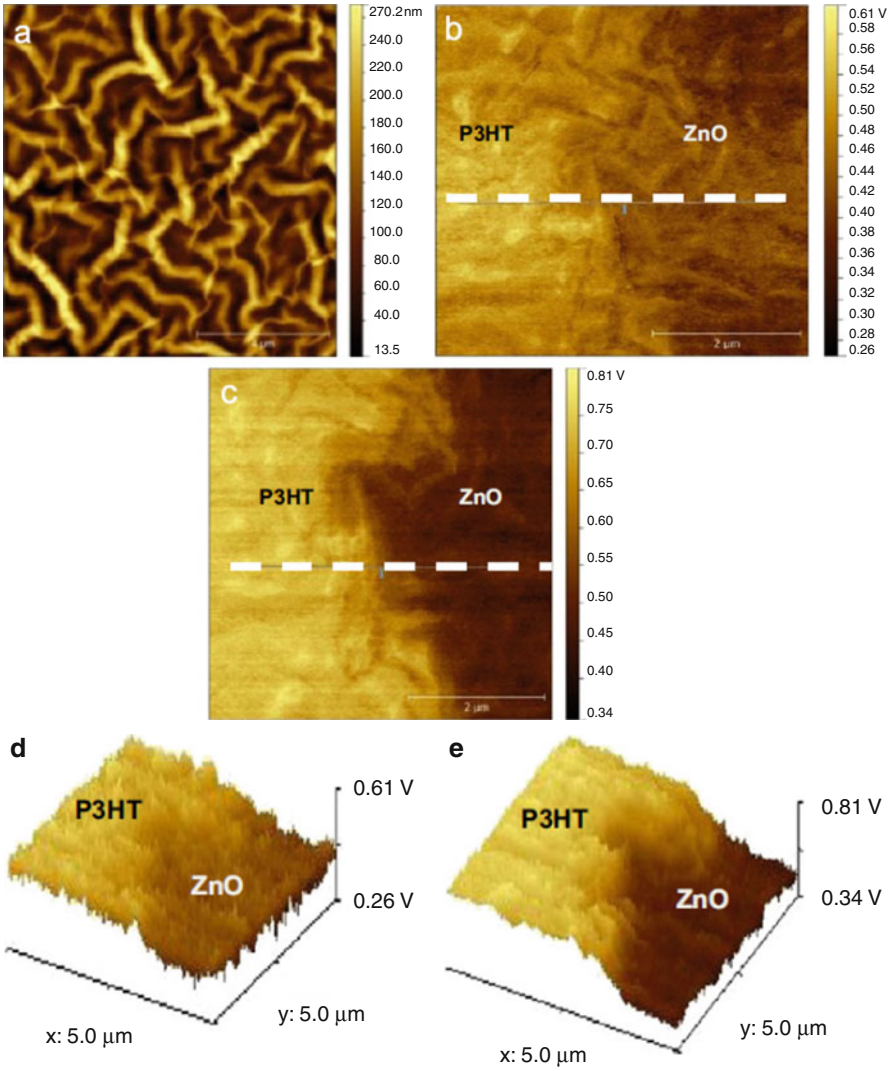

Fig. 20.19 (continued)

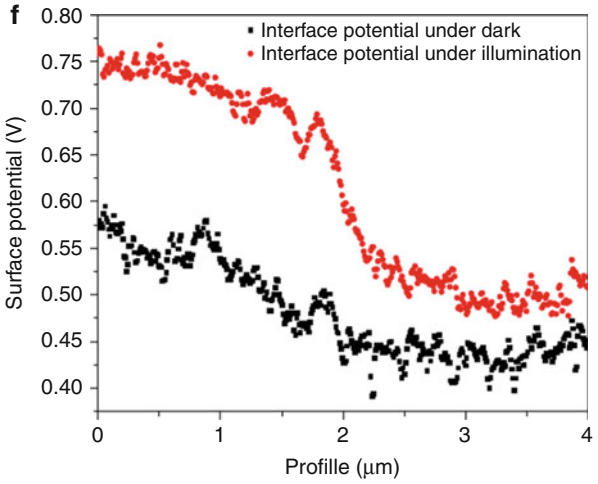

Fig. 20.19 (**a**) AFM image showing ZnO nanoridge topography; surface potential image of P3HT/ZnO film in (**b**) dark condition and (**c**) illuminated condition; 3D SP image of P3HT/ZnO film in (**d**) dark condition and (**e**) illuminated condition; cross-section profile of SP in the film (Reproduced with permission from Ref. [189])

LUMO of PCBM, therefore it shows little probability of electron transfer from PCBM to Nb_2O_5. However, Nb_2O_5-based device showed an efficiency of 2.7 %, suggesting that electron transport to electrode takes place through tunneling. Therefore, as film thickness increased, tunneling distance also increased, thus inhibiting electron transport to the electrode.

Later in 2012, Siddiki et al. reported use of Nb_2O_5 as electron transport layer in double junction polymer solar cell [11]. Double junction polymer solar cell was fabricated with structure shown in Fig. 20.20a. Nb_2O_5 was used as an interfacial layer for electron transport between front and back cell. 25 nm thick Nb_2O_5 film showed >90 % transmittance in the visible region. J-V characteristics of double junction cell and individual cells are shown in Fig. 20.20b. Device efficiency of double junction cell was found to be 0.8 % with a V_{oc} of 1.3 V, which was higher than individual front and back cells. The J_{sc} of double junction solar cell is less than the individual cells. The series resistance was also found to be increased in the double junction cell. The decrease in J_{sc} and increase of series resistance were possibly caused by two factors: (1) mismatch in current between front and back cells and (2) barrier formed at the interfacial layer between the two cells. The higher V_{oc} indicated Nb_2O_5 can be used as electron transport layer in double junction polymer solar cells. Simulation results showed that device performance using Nb_2O_5 could be improved by current matching of individual cells and reducing series resistance.

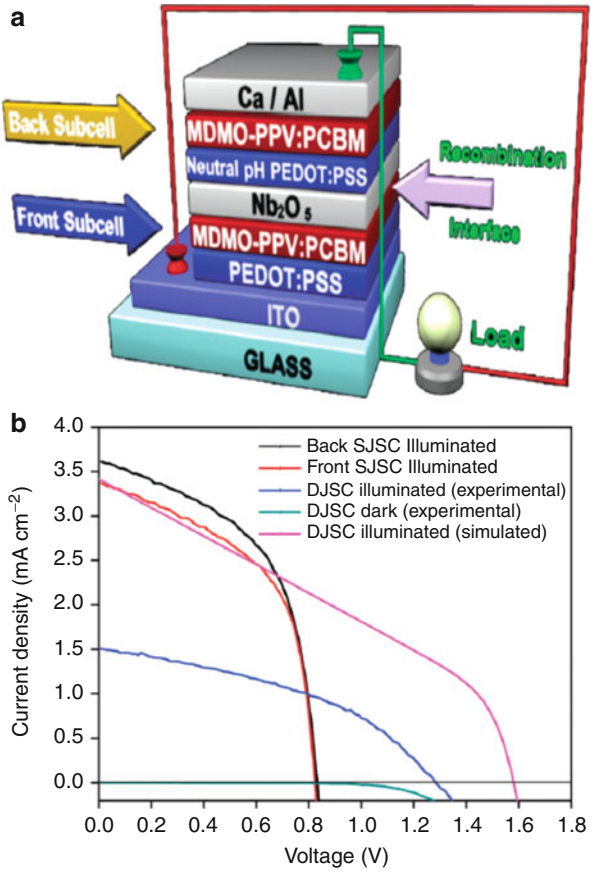

Fig. 20.20 (**a**) Device structure of double junction polymer solar cells and (**b**) J-V plots of front cell, back cell, double junction solar cell (Reproduced from Ref. [11], with permission from the PCCP Owner Societies.)

CuO

Copper oxide has been recently used as interfacial layer to improve the stability in polymer solar cells. Wang et al. in 2011 fabricated polymer bulk heterojunction solar cells by introducing CuO_x layer in between cathode and P3HT:PCBM [10]. Two device structures were fabricated: one with a thin layer (~5 nm) of CuO_x which was deposited by thermal evaporation in a structure of ITO/PEDOT:PSS/P3HT:PCBM/CuO_x/Al and the other was a bilayer of CuO_x and LiF in a device structure of ITO/PEDOT:PSS/P3HT:PCBM/LiF/CuO_x/Al and ITO/PEDOT:PSS/P3HT:PCBM/CuO_x/LiF/Al.

The thickness of LiF was 0.6 nm. The devices without CuO_x interfacial layer showed an efficiency of 1.5 %, while that using CuO_x as interfacial layer exhibited a similar efficiency but a higher J_{sc} and lower V_{oc}. Decrease in V_{oc} was attributed to the high work function of CuO_x in comparison to aluminum. On the other hand,

devices fabricated using a bilayer of CuO_x/LiF showed improvement in V_{oc}. Introduction of CuO_x improved device stability, but did not show improvement in device performance. Device stability was monitored by keeping the devices made without and with CuO_x in air. Devices without CuO_x layer showed ~50 % efficiency decrease after 3 h in air, which was mainly due to decrease in J_{sc}. The devices made using CuO_x/LiF exhibited a 40 % efficiency increase, which was probably due to increase in V_{oc} and FF when kept in air. The increase in V_{oc} and FF was attributed to the oxidation of CuO_x in air, leading to increase in shunt resistance and reduction of quenching of excitons and charge carriers occurring at the metal cathode. Device with CuO_x layers retained ~80 % of the initial efficiency after 240 h and ~50 % after 500 h. Therefore, it was concluded that use of LiF and CuO_x improved charge collection and increased V_{oc} and FF of devices.

Conclusion

General synthesis methods of common nanomaterials including TiO_2, ZnO, Nb_2O_5, and CuO with 0D, 1D, 2D, and 3D hierarchical nanostructures and their applications in solar cells have been reviewed in this chapter. Although laboratory-based synthesis methods have been extensively developed, there are still few methods that can realize large-scale, low-cost, and environmental-friendly synthesis processing, especially for the synthesis of some specific structures, such as TiO_2 and ZnO nanoarrays. However, applications usually require metal oxides have special structures with aimed properties. For TiO_2 and ZnO films used in polymer-inorganic hybrid solar cells as efficient electron transport layer, high crystallinity and surface area are required to facilitate charge separation and transport. Thus, design of ideal structures with large-scale synthesis capability is one of the largest missions of inorganic synthetic chemistry. Nanostructured metal oxides have played an important role in improving polymer-inorganic hybrid solar cell performance. These inorganic metal oxides possess high charge mobility, solution processability, and are environmentally stable. Therefore introduction of metal oxides into solar cells has led to improvement in performance of polymer-inorganic hybrid solar cells. Nanostructured metal oxides have brought new design and properties in fabricating solar cells.

Acknowledgement This work was supported in part by NSF CAREER (ECCS-0950731), NSF EPSCoR (Grant No. 0903804), and the State of South Dakota, NASA EPSCoR (No. NNX13AD31A), 3 M Nontenured Faculty Award, and SDBoR CRGP grant.

References

1. Alparslan Z, Kosemen A, Ornek O et al (2011) TiO_2-based organic hybrid solar cells withMn^{+2} doping. Int J Photoenergy
2. Breeze AJ, Schlesinger Z, Carter SA (2001) Charge transport in TiO_2/MEH-PPV polymer photovoltaics. Phys Rev B 64(125205):1–9

3. Bouclé J, Chyla S, Shaffer MSP et al (2008) Hybrid solar cells from a blend of poly (3-hexylthiophene) and ligand-capped TiO_2 nanorods. Adv Funct Mater 18(4):622–633
4. Chang C-H, Huang T-K, Lin Y-T et al (2008) Improved charge separation and transport efficiency in poly(3-hexylthiophene)–TiO_2 nanorod bulk heterojunction solar cells. J Mater Chem 18(19):2201–2207
5. Liang S, Zhu G, Wenbin G, Chen T, Xindong Z, Caixia L, Weiyou C, Shengping R, Zhicheng Z (2008) Performance improvement of TiO_2/P3HT solar cells using CuPc as a sensitizer. Appl Phys Lett 92(7):073307
6. Beek WJE, Slooff LH, Wienk MM et al (2005) Hybrid ZnO: polymer bulk heterojunction solar cells from a ZnO precursor. In: Organic photovoltaics VI. SPIE
7. Beek W, Wienk M, Janssen R (2006) Hybrid solar cells from regioregular polythiophene and ZnO nanoparticles. Adv Funct Mater 16(8):1112–1116
8. Beek WJE, Wienk MM, Janssen RAJ (2005) Hybrid bulk heterojunction solar cells: blends of ZnO semiconducting nanoparticles and conjugated polymers. In: Organic photovoltaics VI. SPIE
9. Kuwabara T, Kawahara Y, Yamaguchi T et al (2009) Characterization of inverted-type organic solar cells with a ZnO layer as the electron collection electrode by ac impedance spectroscopy. ACS Appl Mater Interfaces 1(10):2107–2110
10. Wang M, Xie F, Xie W et al (2011) Device lifetime improvement of polymer-based bulk heterojunction solar cells by incorporating copper oxide layer at Al cathode. Appl Phys Lett 98(18):183304
11. Siddiki MK, Venkatesan S, Qiao Q (2012) Nb_2O_5 as a new electron transport layer for double junction polymer solar cells. Phys Chem Chem Phys 14(14):4682–4686
12. Chen X, Mao SS (2007) Titanium dioxide nanomaterials: synthesis, properties, modifications, and applications. Chem Rev 107(7):2891–2959
13. Chen H, Nanayakkara C, Grassian V (2012) Titanium dioxide photocatalysis in atmospheric chemistry. Chem Rev 112(11):5919–5948
14. Biswas P, Kundu S, Banerji P (2013) A study on electrical transport vis-a-vis the effect of thermal annealing on the p-type conductivity in arsenic-doped MOCVD grown ZnO in the temperature range 10–300 K. J Alloys Compd 552:304–309
15. Liu CY, Zhang BP, Binh NT et al (2006) Temperature dependence of structural and optical properties of ZnO films grown on Si substrates by MOCVD. J Cryst Growth 290(2):314–318
16. Pradhan SK, Reucroft PJ, Yang FQ et al (2003) Growth of TiO_2 nanorods by metalorganic chemical vapor deposition. J Cryst Growth 256(1–2):83–88
17. Liu B, Hu Z, Che Y et al (2008) Growth of ZnO nanoparticles and nanorods with ultrafast pulsed laser deposition. Appl Phys A Mater Sci Process 93(3):813–818
18. Limmer SJ, Seraji S, Wu Y et al (2002) Template-based growth of various oxide nanorods by sol-gel electrophoresis. Adv Funct Mater 12(1):59–64
19. Antonelli DM, Ying JY (1995) Synthesis of hexagonally packed mesoporous TiO_2 by a modified sol-gel method. Angew Chem Int Ed 34(18):2014–2017
20. Lakshmi BB, Patrissi CJ, Martin CR (1997) Sol-gel template synthesis of semiconductor oxide micro- and nanostructures. Chem Mater 9(11):2544–2550
21. Yanan F, Zhengguo J, Weijiang X et al (2008) Ordered macro-mesoporous nc-TiO_2 films by sol-gel method using polystyrene array and triblock copolymer bitemplate. J Am Ceram Soc 91(8):2676–2682
22. Spanhel L, Anderson MA (1991) Semiconductor clusters in the sol-gel process: quantized aggregation, gelation, and crystal growth in concentrated zinc oxide colloids. J Am Chem Soc 113(8):2826–2833
23. Rahnama A, Gharagozlou M (2012) Preparation and properties of semiconductor CuO nanoparticles via a simple precipitation method at different reaction temperatures. Opt Quant Electron 44(6–7):313–322
24. Bavykin DV, Parmon VN, Lapkin AA et al (2004) The effect of hydrothermal conditions on the mesoporous structure of TiO_2 nanotubes. J Mater Chem 14(22):3370–3377

25. Andersson M, Osterlund L, Ljungstrom S et al (2002) Preparation of nanosize anatase and rutile TiO_2 by hydrothermal treatment of microemulsions and their activity for photocatalytic wet oxidation of phenol. J Phys Chem B 106(41):10674–10679
26. Wu MM, Long JB, Huang AH et al (1999) Microemulsion-mediated hydrothermal synthesis and characterization of nanosize rutile and anatase particles. Langmuir 15(26):8822–8825
27. Guixiang D, Lidong Z, Yan F et al (2012) Controllable synthesis of ZnO architectures by a surfactant-free hydrothermal process. Mater Lett 73:86–88
28. Yang J, Mei S, Ferreira JMF (2001) Hydrothermal synthesis of TiO_2 nanopowders from tetraalkylammonium hydroxide peptized sols. Mater Sci Eng C-Biomimetic Supramol Syst 15(1–2):183–185
29. Patil KC, Aruna ST, Ekambaram S (1997) Combustion synthesis. Curr Opin Solid State Mater Sci 2(2):158–165
30. Nagaveni K, Hegde MS, Madras G (2004) Structure and photocatalytic activity of $Ti_{1-x}M_xO_{2\pm\delta}$ (M = W, V, Ce, Zr, Fe, and Cu) synthesized by solution combustion method. J Phys Chem B 108(52):20204–20212
31. Jimenez-Gonzalez AE, Urueta JAS, Suarez-Parra R (1998) Optical and electrical characteristics of aluminum-doped ZnO thin films prepared by solgel technique. J Cryst Growth 192(3–4):430–438
32. Cong Y, Zhang J, Chen F et al (2007) Synthesis and characterization of nitrogen-doped TiO_2 nanophotocatalyst with high visible light activity. J Phys Chem C 111(19):6976–6982
33. Elias J, Levy-Clement C, Bechelany M et al (2010) Hollow Urchin-like ZnO thin films by electrochemical deposition. Adv Mater 22(14):1607–+
34. Roy P, Berger S, Schmuki P (2011) TiO_2 nanotubes: synthesis and applications. Angew Chem Int Ed 50(13):2904–2939
35. Kong M, Zhang W, Yang Z et al (2011) Facile synthesis of CuO hollow nanospheres assembled by nanoparticles and their electrochemical performance. Appl Surf Sci 258(4):1317–1321
36. Kafi AKM, Wu G, Chen A (2008) A novel hydrogen peroxide biosensor based on the immobilization of horseradish peroxidase onto Au-modified titanium dioxide nanotube arrays. Biosens Bioelectron 24(4):566–571
37. Izaki M, Watanabe M, Aritomo H et al (2008) Zinc oxide nano-cauliflower array with room temperature ultraviolet light emission. Cryst Growth Des 8(4):1418–1421
38. Xu J, Yang X, Yang QD et al (2012) Arrays of CdSe sensitized ZnO/ZnSe nanocables for efficient solar cells with high open-circuit voltage. J Mater Chem 22(26):13374–13379
39. Sakthivel S, Janczarek M, Kisch H (2004) Visible light activity and photoelectrochemical properties of nitrogen-doped TiO_2. J Phys Chem B 108(50):19384–19387
40. Zhang X, Wang G, Zhang W et al (2008) Seed-mediated growth method for epitaxial array of CuO nanowires on surface of Cu nanostructures and its application as a glucose sensor. J Phys Chem C 112(24):8856–8862
41. Kongkanand A, Tvrdy K, Takechi K et al (2008) Quantum dot solar cells. Tuning photoresponse through size and shape control of CdSe-TiO_2 architecture. J Am Chem Soc 130(12):4007–4015
42. Cho IS, Chen Z, Forman AJ et al (2011) Branched TiO_2 nanorods for photoelectrochemical hydrogen production. Nano Lett 11(11):4978–4984
43. Zhang Z, Zhang L, Hedhili M et al (2013) Plasmonic gold nanocrystals coupled with photonic crystal seamlessly on TiO_2 nanotube photoelectrodes for efficient visible light photoelectrochemical water splitting. Nano Lett 13(1):14–20
44. Zhu K, Neale NR, Miedaner A et al (2007) Enhanced charge-collection efficiencies and light scattering in dye-sensitized solar cells using oriented TiO_2 nanotubes arrays. Nano Lett 7(1):69–74
45. Fujishima A, Honda K (1972) Electrochemical photolysis of water at a semiconductor electrode. Nature 238(5358):37–38

46. Zeng HB, Cui JB, Cao BQ et al (2010) Electrochemical deposition of ZnO nanowire arrays: organization, doping, and properties. Sci Adv Mater 2(3):336–358
47. Fujishima A, Zhang X, Tryk DA (2008) TiO_2 photocatalysis and related surface phenomena. Surf Sci Rep 63(12):515–582
48. Inoue T, Fujishima A, Konishi S et al (1979) Photoelectrocatalytic reduction of carbon dioxide in aqueous suspensions of semiconductor powders. Nature 277(5698):637–638
49. Law M, Greene LE, Johnson JC et al (2005) Nanowire dye-sensitized solar cells. Nat Mater 4(6):455–459
50. O'Regan B, Gratzel M (1991) A low-cost, high-efficiency solar cell based on dye-sensitized colloidal TiO_2 films. Nature 353(6346):737–740
51. Senthilarasu S, Peiris TAN, Jorge G-C et al (2012) Preparation of nanocrystalline TiO_2 electrodes for flexible dye-sensitized solar cells: influence of mechanical compression. J Phys Chem C 116:19053–19061
52. Bao S-J, Li CM, Zang J-F et al (2008) New nanostructured TiO_2 for direct electrochemistry and glucose sensor applications. Adv Funct Mater 18(4):591–599
53. Sakthivel S, Kisch H (2003) Daylight photocatalysis by carbon-modified titanium dioxide. Angew Chem Int Ed 42(40):4908–4911
54. Su W, Zhang Y, Li Z et al (2008) Multivalency iodine doped TiO_2: preparation, characterization, theoretical studies, and visible-light photocatalysis. Langmuir 24(7):3422–3428
55. Varley J, Janotti A, Van de Walle C (2011) Mechanism of visible-light photocatalysis in nitrogen-doped TiO_2. Adv Mater 23(20):2343–2347
56. Li Z, Zhang H, Zheng W et al (2008) Highly sensitive and stable humidity nanosensors based on LiCl doped TiO_2 electrospun nanofibers. J Am Chem Soc 130(15):5036–+
57. Lu C, Chen Z (2009) High-temperature resistive hydrogen sensor based on thin nanoporous rutile TiO(2) film on anodic aluminum oxide. Sensor Actuat B-chem 140(1):109–115
58. Lu HF, Li F, Liu G et al (2008) Amorphous TiO(2) nanotube arrays for low-temperature oxygen sensors. Nanotechnology 19(40)
59. Yang L, Luo S, Cai Q et al (2010) A review on TiO_2 nanotube arrays: fabrication, properties, and sensing applications. Chin Sci Bull 55(4–5):331–338
60. Zhang Y, Fu W, Yang H et al (2008) Synthesis and characterization of TiO(2) nanotubes for humidity sensing. Appl Surf Sci 254(17):5545–5547
61. Kim JY, Kim SH, Lee HH et al (2006) New architecture for high-efficiency polymer photovoltaic cells using solution-based titanium oxide as an optical spacer. Adv Mater 18(5):572–+
62. Kokubo T, Kim HM, Kawashita M (2003) Novel bioactive materials with different mechanical properties. Biomaterials 24(13):2161–2175
63. Chae SY, Park MK, Lee SK et al (2003) Preparation of size-controlled TiO_2 nanoparticles and derivation of optically transparent photocatalytic films. Chem Mater 15(17):3326–3331
64. Yu JC, Yu JG, Ho WK et al (2002) Effects of F-doping on the photocatalytic activity and microstructures of nanocrystalline TiO_2 powders. Chem Mater 14(9):3808–3816
65. Carp O, Huisman CL, Reller A (2004) Photoinduced reactivity of titanium dioxide. Prog Solid State Chem 32(1–2):33–177
66. Cot F, Larbot A, Nabias G et al (1998) Preparation and characterization of colloidal solution derived crystallized titania powder. J Eur Ceram Soc 18(14):2175–2181
67. Pinna N, Niederberger M (2008) Surfactant-free nonaqueous synthesis of metal oxide nanostructures. Angew Chem Int Ed 47(29):5292–5304
68. Li XL, Peng Q, Yi JX et al (2006) Near monodisperse TiO_2 nanoparticles and nanorods. Chem Eur J 12(8):2383–2391
69. Shah SI, Li W, Huang CP et al (2002) Study of Nd3+, Pd2+, Pt4+, and Fe3+ dopant effect on photoreactivity of TiO_2 nanoparticles. Proc Natl Acad Sci USA 99:6482–6486
70. Chen C-A, Chen Y-M, Huang Y-S et al (2009) Synthesis and characterization of well-aligned anatase TiO_2 nanocrystals on fused silica via metal-organic vapor deposition. Cryst Eng Comm 11(11):2313–2318

71. Yang HG, Sun CH, Qiao SZ et al (2008) Anatase TiO(2) single crystals with a large percentage of reactive facets. Nature 453(7195):638-U4
72. Li GS, Li LP, Boerio-Goates J et al (2005) High purity anatase TiO_2 nanocrystals: near room-temperature synthesis, grain growth kinetics, and surface hydration chemistry. J Am Chem Soc 127(24):8659–8666
73. Burnside SD, Shklover V, Barbe C et al (1998) Self-organization of TiO_2 nanoparticles in thin films. Chem Mater 10(9):2419–2425
74. Sugimoto T, Zhou XP, Muramatsu A (2003) Synthesis of uniform anatase TiO_2 nanoparticles by gel-sol method 3. Formation process and size control. J Colloid Interface Sci 259(1):43–52
75. Sugimoto T, Zhou XP, Muramatsu A (2003) Synthesis of uniform anatase TiO_2 nanoparticles by gel-sol method 4. Shape control. J Colloid Interface Sci 259(1):53–61
76. Sugimoto T, Zhou XP, Muramatsu A (2002) Synthesis of uniform anatase TiO_2 nanoparticles by gel-sol method – 1. Solution chemistry of Ti(OH)(n)((4-n)+) complexes. J Colloid Interface Sci 252(2):339–346
77. Sugimoto T, Zhou XP (2002) Synthesis of uniform anatase TiO_2 nanoparticles by the gel-sol method – 2. Adsorption of OH- ions to Ti(OH)(4) gel and TiO_2 particles. J Colloid Interface Sci 252(2):347–353
78. Sugimoto T, Okada K, Itoh H (1997) Synthesis of uniform spindle-type titania particles by the gel-sol method. J Colloid Interface Sci 193(1):140–143
79. Fu G, Vary P, Lin C-T (2005) Anatase TiO_2 nanocomposites for antimicrobial coatings. J Phys Chem B 109(18):8889–8898
80. Kasuga T, Hiramatsu M, Hoson A et al (1998) Formation of titanium oxide nanotube. Langmuir 14(12):3160–3163
81. Zhong ZY, Yin YD, Gates B et al (2000) Preparation of mesoscale hollow spheres of TiO_2 and SnO_2 by templating against crystalline arrays of polystyrene beads. Adv Mater 12(3):206–+
82. Qiao QQ, McLeskey JT (2005) Water-soluble polythiophene/nanocrystalline TiO_2 solar cells. Appl Phys Lett 86(15):153501
83. Xu T, Yan M, Hoefelmeyer JD et al (2012) Exciton migration and charge transfer in chemically linked P3HT-TiO_2 nanorod composite. RSC Adv 2(3):854–862
84. Kang SH, Choi S-H, Kang M-S et al (2008) Nanorod-based dye-sensitized solar cells with improved charge collection efficiency. Adv Mater 20(1):54–+
85. Cozzoli PD, Kornowski A, Weller H (2003) Low-temperature synthesis of soluble and processable organic-capped anatase TiO_2 nanorods. J Am Chem Soc 125(47):14539–14548
86. Wu J-M (2004) Low-temperature preparation of titania nanorods through direct oxidation of titanium with hydrogen peroxide. J Cryst Growth 269(2–4):347–355
87. Liu B, Aydil ES (2009) Growth of oriented single-crystalline rutile TiO_2 nanorods on transparent conducting substrates for dye-sensitized solar cells. J Am Chem Soc 131(11):3985–3990
88. Hoyer P (1996) Formation of a titanium dioxide nanotube array. Langmuir 12(6):1411–1413
89. Daoai W, Tianchang H, Litian H et al (2009) Microstructured arrays of TiO_2 nanotubes for improved photo-electrocatalysis and mechanical stability. Adv Funct Mater 19
90. Tsai C, Teng H (2006) Structural features of nanotubes synthesized from NaOH treatment on TiO_2 with different post-treatments. Chem. Mater 18(2):367–373
91. Lan Y, Gao XP, Zhu HY et al (2005) Titanate nanotubes and nanorods prepared from rutile powder. Adv Funct Mater 15(8):1310–1318
92. Tian ZRR, Voigt JA, Liu J et al (2003) Large oriented arrays and continuous films of TiO_2-based nanotubes. J Am Chem Soc 125(41):12384–12385
93. Macak JM, Tsuchiya H, Schmuki P (2005) High-aspect-ratio TiO_2 nanotubes by anodization of titanium. Angew Chem Int Ed 44(14):2100–2102
94. Jan MM, Cordt Z, Brian JR et al (2009) Ordered ferroelectric lead titanate nanocellular structure by conversion of anodic TiO_2 nanotubes. Adv Mater 21:3121–3125

95. Mor GK, Shankar K, Paulose M et al (2006) Use of highly-ordered TiO_2 nanotube arrays in dye-sensitized solar cells. Nano Lett 6(2):215–218
96. Bavykin DV, Friedrich JM, Walsh FC (2006) Protonated titanates and TiO_2 nanostructured materials: synthesis, properties, and applications. Adv Mater 18(21):2807–2824
97. Yuan ZY, Zhou WZ, Su BL (2002) Hierarchical interlinked structure of titanium oxide nanofibers. Chem Commun 2(11):1202–1203
98. Joshi P, Zhang L, Davoux D et al (2010) Composite of TiO_2 nanofibers and nanoparticles for dye-sensitized solar cells with significantly improved efficiency. Energy Environ Sci 3(10):1507–1510
99. Qidong T, Xingzhong Z, Feng Y (2010) Hybrid solar cells based on poly(3-hexylthiophene) and electrospun TiO_2 nanofibers with effective interface modification. J Mater Chem 20:7366–7371
100. Drew C, Liu X, Ziegler D et al (2003) Metal oxide-coated polymer nanofibers. Nano Lett 3(2):143–147
101. Li D, Xia YN (2003) Fabrication of titania nanofibers by electrospinning. Nano Lett 3(4):555–560
102. Li D, Xia YN (2003) Rapid fabrication of titania nanofibers by electrospinning. In: Cao G, Xia Y, Braun PV (eds) Nanomaterials and their optical applications. pp 17–24
103. Choi W, Termin A, Hoffmann MR (1994) The role of metal ion dopants in quantum-sized TiO_2: correlation between photoreactivity and charge carrier recombination dynamics. J Phys Chem 98(51):13669–13679
104. Gole JL, Stout JD, Burda C et al (2003) Highly efficient formation of visible light tunable $TiO_{2-x}N_x$ photocatalysts and their transformation at the nanoscale. J Phys Chem B 108(4):1230–1240
105. Park JH, Kim S, Bard AJ (2005) Novel carbon-doped TiO_2 nanotube arrays with high aspect ratios for efficient solar water splitting. Nano Lett 6(1):24–28
106. Burda C, Lou Y, Chen X et al (2003) Enhanced nitrogen doping in TiO_2 nanoparticles. Nano Lett 3(8):1049–1051
107. Ohno T (2004) Preparation of visible light active S-doped TiO_2 photocatalysts and their photocatalytic activities. Water Sci Technol 49(4):159–163
108. Luo H, Takata T, Lee Y et al (2004) Photocatalytic activity enhancing for titanium dioxide by co-doping with bromine and chlorine. Chem Mater 16(5):846–849
109. Hsieh CY, Lu ML, Chen JY et al (2012) Single ZnO nanowire-PZT optothermal field effect transistors. Nanotechnology 23(35)
110. Yang M, Kim HC, Hong SH (2012) DMMP gas sensing behavior of ZnO-coated single-wall carbon nanotube network sensors. Mater Lett 89:312–315
111. Xu CK, Wu JM, Desai UV et al (2012) High-efficiency solid-state dye-sensitized solar cells based on TiO_2-coated ZnO nanowire arrays. Nano Lett 12(5):2420–2424
112. Tingting X, Qiquan Q (2011) Conjugated polymer–inorganic semiconductor hybrid solar cells. Energy Environ Sci 4:2700–2720
113. Shangke P, Tingting X, Swaminathan V et al (2012) Direct growth of CdSe nanorods on ITO substrates by co-anchoring of ZnO nanoparticles and ethylenediamine. J Nanopart Res 14:1115
114. Xie Y, Joshi P, Darling SB et al (2010) Electrolyte effects on electron transport and recombination at ZnO nanorods for dye-sensitized solar cells. J Phys Chem C 114(41):17880–17888
115. Tingting X, Swaminathan V, David G et al (2013) Study of polymer/ZnO nanostructure interfaces by Kelvin probe force microscopy. Sol Energy Mater Sol Cells 108:246–251
116. Afsal M, Wang CY, Chu LW et al (2012) Highly sensitive metal-insulator-semiconductor UV photodetectors based on ZnO/SiO_2 core-shell nanowires. J Mater Chem 22(17):8420–8425
117. Gao PX, Song JH, Liu J et al (2007) Nanowire piezoelectric nanogenerators on plastic substrates as flexible power sources for nanodevices. Adv Mater 19(1):67–+
118. Soomro MY, Hussain I, Bano N et al (2012) Piezoelectric power generation from zinc oxide nanowires grown on paper substrate. Phys Status Solidi-R 6(2):80–82

119. Kawano T, Imai H (2010) Nanoscale morphological design of ZnO crystals grown in aqueous solutions. J Ceram Soc Jpn 118(1383):969–976
120. Wang XD, Summers CJ, Wang ZL (2004) Large-scale hexagonal-patterned growth of aligned ZnO nanorods for nano-optoelectronics and nanosensor arrays. Nano Lett 4(3):423–426
121. Chen JJ, Gao Y, Zeng F et al (2004) Effect of sputtering oxygen partial pressures on structure and physical properties of high resistivity ZnO films. Appl Surf Sci 223(4):318–329
122. Hu Z, Oskam G, Searson PC (2003) Influence of solvent on the growth of ZnO nanoparticles. J Colloid Interface Sci 263(2):454–460
123. Yadav RS, Mishra P, Pandey AC (2008) Growth mechanism and optical property of ZnO nanoparticles synthesized by sonochemical method. Ultrason Sonochem 15(5):863–868
124. Kawano T, Imai H (2006) Fabrication of ZnO nanoparticles with various aspect ratios through acidic and basic routes. Cryst Growth Des 6(4):1054–1056
125. Distaso M, Klupp Taylor RN, Taccardi N et al (2011) Influence of the counterion on the synthesis of ZnO mesocrystals under solvothermal conditions. Chemistry 17(10):2923–2930
126. Jézéquel D, Guenot J, Jouini N et al (1995) Submicrometer zinc oxide particles: elaboration in polyol medium and morphological characteristics. J Mater Res 10(01):77–83
127. Zhang Q, Chou T, Russo B et al (2008) Aggregation of ZnO nanocrystallites for high conversion efficiency in dye-sensitized solar cells. Angew Chem Int Ed 47(13):2402–2406
128. Shinde SS, Korade AP, Bhosale CH et al (2013) Influence of tin doping onto structural, morphological, optoelectronic and impedance properties of sprayed ZnO thin films. J Alloys Compd 551:688–693
129. Chen Y-Y, Hsu J-C, Lee C-Y et al (2013) Influence of oxygen partial pressure on structural, electrical, and optical properties of Al-doped ZnO film prepared by the ion beam co-sputtering method. J Mater Sci 48(3):1225–1230
130. Ramgir NS, Late DJ, Bhise AB et al (2006) ZnO multipods, submicron wires, and spherical structures and their unique field emission behavior. J Phys Chem B 110(37):18236–18242
131. Ng HT, Chen B, Li J et al (2003) Optical properties of single-crystalline ZnO nanowires on m-sapphire. Appl Phys Lett 82(13):2023–2025
132. Lee WN, Jeong MC, Myoung JM (2004) Fabrication and application potential of ZnO nanowires grown on GaAs(002) substrates by metal-organic chemical vapour deposition. Nanotechnology 15(3):254–259
133. Ramsdale CM, Greenham NC (2002) Ellipsometric determination of anisotropic optical constants in electroluminescent conjugated polymers. Adv Mater 14(3):212–+
134. Vayssieres L (2003) Growth of arrayed nanorods and nanowires of ZnO from aqueous solutions. Adv Mater 15(5):464–466
135. Greene LE, Law M, Tan DH et al (2005) General route to vertical ZnO nanowire arrays using textured ZnO seeds. Nano Lett 5(7):1231–1236
136. Xu TT, Chen QL, Lin DH et al (2011) Self-assembled thienylsilane molecule as interfacial layer for ZnO nanowire/polymer hybrid system. J Photonics Energy 1(1):011107
137. Hu P, Liu YQ, Wang XB et al (2003) Tower-like structure of ZnO nanocolumns. Chem Commun 3(11):1304–1305
138. Wang Z, Qian XF, Yin J et al (2004) Large-scale fabrication of tower-like, flower-like, and tube-like ZnO arrays by a simple chemical solution route. Langmuir 20(8):3441–3448
139. Liang Y, Zhang X, Qin L et al (2006) Ga-assisted synthesis and optical properties of ZnO submicron- and nanotowers. J Phys Chem B 110(43):21593–21595
140. Xiao J, Zhang X, Zhang G (2008) Field emission from zinc oxide nanotowers: the role of the top morphology. Nanotechnology 19(29):295706
141. Wang F, Cao L, Pan A et al (2007) Synthesis of tower-like ZnO structures and visible photoluminescence origins of varied-shaped ZnO nanostructures. J Phys Chem C 111(21):7655–7660

142. Wang WW, Zhu YJ (2004) Shape-controlled synthesis of zinc oxide by microwave heating using an imidazolium salt. Inorg Chem Commun 7(9):1003–1005
143. Gao XD, Li XM, Yu WD (2005) Flowerlike ZnO nanostructures via hexamethylenetetramine-assisted thermolysis of zinc-ethylenediamine complex. J Phys Chem B 109(3):1155–1161
144. Umetsu M, Mizuta M, Tsumoto K et al (2005) Bioassisted room-temperature immobilization and mineralization of zinc oxide – the structural ordering of ZnO nanoparticles into a flower-type morphology. Adv Mater 17(21):2571–+
145. Li P, Liu H, Zhang Y-F et al (2007) Synthesis of flower-like ZnO microstructures via a simple solution route. Mater Chem Phys 106(1):63–69
146. Wahab R, Ansari SG, Kim YS et al (2007) Low temperature solution synthesis and characterization of ZnO nano-flowers. Mater Res Bull 42(9):1640–1648
147. Peng WQ, Qu SC, Cong GW et al (2006) Synthesis and structures of morphology-controlled ZnO nano- and microcrystals. Cryst Growth Des 6(6):1518–1522
148. Xie Q, Dai Z, Liang HB et al (2005) Synthesis of ZnO three-dimensional architectures and their optical properties. Solid State Commun 136(5):304–307
149. Sun F, Qiao X, Tan F et al (2012) Fabrication and photocatalytic activities of ZnO arrays with different nanostructures. Appl Surf Sci 263:704–711
150. Fang Z, Tang K, Shen G et al (2006) Self-assembled ZnO 3D flowerlike nanostructures. Mater Lett 60(20):2530–2533
151. Ye CH, Fang XS, Hao YF et al (2005) Zinc oxide nanostructures: Morphology derivation and evolution. J Phys Chem B 109(42):19758–19765
152. Ozgur U, Alivov YI, Liu C et al (2005) A comprehensive review of ZnO materials and devices. J Appl Phys 98(4):41301
153. Tran VT, Shinya M (2010) Synthesis of high-quality Al-doped ZnO nanoink. J Appl Phys 107:014308
154. Pearton SJ, Heo WH, Ivill M et al (2004) Dilute magnetic semiconducting oxides. Semicond Sci Technol 19(10):R59–R74
155. Park CH, Zhang SB, Wei SH (2002) Origin of p-type doping difficulty in ZnO: the impurity perspective. Phys Rev B 66(7):073202(1-3)
156. Matsumoto Y, Murakami M, Jin ZW et al (1999) Combinatorial laser molecular beam epitaxy (MBE) growth of Mg-Zn-O alloy for band gap engineering. Jpn J Appl Phys Part 2 38(6AB):L603–L605
157. Liu W-S, Chen W-K, Hsueh K-P (2013) Transparent conductive Ga-doped $Mg_xZn_{1-x}O$ films with high optical transmittance prepared by radio frequency magnetron sputtering. J Alloys Compd 552:255–263
158. Wan Q, Li QH, Chen YJ et al (2004) Positive temperature coefficient resistance and humidity sensing properties of Cd-doped ZnO nanowires. Appl Phys Lett 84(16):3085–3087
159. Wang YS, Thomas PJ, O'Brien P (2006) Optical properties of ZnO nanocrystals doped with Cd, Mg, Mn, and Fe ions. J Phys Chem B 110(43):21412–21415
160. Fernandes GE, Lee D-J, Kim JH et al (2013) Infrared and microwave shielding of transparent Al-doped ZnO superlattice grown via atomic layer deposition. J Mater Sci 48(6):2536–2542
161. Kumar S, Chen CL, Dong CL et al (2013) Structural, optical, and magnetic characterization of Co and N co-doped ZnO nanopowders. J Mater Sci 48(6):2618–2623
162. Zhou Y, Qiu Z, Lü M et al (2008) Preparation and characterization of porous Nb_2O_5 nanoparticles. Mater Res Bull 43(6):1363–1368
163. Uekawa N, Kudo T, Mori F et al (2003) Low-temperature synthesis of niobium oxide nanoparticles from peroxo niobic acid sol. J Colloid Interface Sci 264(2):378–384
164. Buha J, Arcon D, Niederberger M et al (2010) Solvothermal and surfactant-free synthesis of crystalline Nb_2O_5, Ta_2O_5, HfO_2, and Co-doped HfO_2 nanoparticles. Phys Chem Chem Phys 12(47):15537–15543
165. Suramwar NV, Thakare SR, Karade NN et al (2012) Green synthesis of predominant (1 1 1) facet CuO nanoparticles: Heterogeneous and recyclable catalyst for N-arylation of indoles. J Mol Catal A Chem 359:28–34

166. Liu S, Tian J, Wang L et al (2012) A simple route for preparation of highly stable CuO nanoparticles for nonenzymatic glucose detection. Catal Sci Technol 2(4):813–817
167. Wang H, Xu J-Z, Zhu J-J et al (2002) Preparation of CuO nanoparticles by microwave irradiation. J Cryst Growth 244(1):88–94
168. Applerot G, Lellouche J, Lipovsky A et al (2012) Understanding the antibacterial mechanism of CuO nanoparticles: revealing the route of induced oxidative stress. Small 8(21):3326–3337
169. Vidyasagar CC, Naik YA, Venkatesh TG et al (2011) Solid-state synthesis and effect of temperature on optical properties of Cu–ZnO, Cu–CdO and CuO nanoparticles. Powder Technol 214(3):337–343
170. Sun L, Zhang Z, Wang Z et al (2005) Synthesis and characterization of CuO nanoparticles from liquid ammonia. Mater Res Bull 40(6):1024–1027
171. Premkumar T, Geckeler KE (2006) A green approach to fabricate CuO nanoparticles. J Phys Chem Solids 67(7):1451–1456
172. Liu B, Zeng HC (2004) Mesoscale organization of CuO nanoribbons: formation of "dandelions". J Am Chem Soc 126(26):8124–8125
173. Chang Y, Teo JJ, Zeng HC (2004) Formation of colloidal CuO nanocrystallites and their spherical aggregation and reductive transformation to hollow Cu_2O nanospheres. Langmuir 21(3):1074–1079
174. Zhu J, Qian X (2010) From 2-D CuO nanosheets to 3-D hollow nanospheres: interface-assisted synthesis, surface photovoltage properties and photocatalytic activity. J Solid State Che 183(7):1632–1639
175. Park JC, Kim J, Kwon H et al (2009) Gram-scale synthesis of Cu_2O nanocubes and subsequent oxidation to CuO hollow nanostructures for lithium-ion battery anode materials. Adv Mater 21(7):803–807
176. Cheng S-L, Chen M-F (2012) Fabrication, characterization, and kinetic study of vertical single-crystalline CuO nanowires on Si substrates. Nanoscale Res Lett 7(1):119
177. Jiang X, Herricks T, Xia Y (2002) CuO nanowires can be synthesized by heating copper substrates in air. Nano Lett 2(12):1333–1338
178. Hansen BJ, Kouklin N, Lu G et al (2010) Transport, Analyte detection, and opto-electronic response of p-type CuO nanowires. J Phys Chem C 114(6):2440–2447
179. Hansen BJ, Lu G, Chen J (2008) Direct oxidation growth of CuO nanowires from copper-containing substrates. J Nanomater 2008:1–7
180. Umar AA, Oyama M (2007) A seed-mediated growth method for vertical array of single-crystalline CuO nanowires on surfaces. Cryst Growth Des 7(12):2404–2409
181. Siddiki M, Li J, Galipeau D et al (2010) A review on polymer multijunction solar cells. Energy Environ Sci 3:867–883
182. Siddiki MK, Venkatesan S, Galipeau D et al (2013) Kelvin probe force microscopic imaging of the energy barrier and energetically favorable offset of interfaces in double-junction organic solar cells. ACS Appl Mater Interfaces 5(4):1279–1286
183. Siddiki MK, Venkatesan S, Wang M et al (2013) Materials and devices design for efficient double junction polymer solar cells. Sol Energy Mater Sol Cells 108:225–229
184. Taranekar P, Qiao Q, Jiang J et al (2007) Hyperbranched conjugated polyelectrolyte bilayers for solar cell applications. J Am Chem Soc 129(29):8958–8959
185. Xie Y, Bao Y, Du J et al (2012) Understanding of morphology evolution in local aggregates and neighboring regions for organic photovoltaics. Phys Chem Chem Phys 14:10168–10177
186. Xie Y, Li Y, Xiao L et al (2010) Femtosecond time-resolved fluorescence study of P3HT/PCBM blend films. J Phys Chem C 114(34):14590–14600
187. Xu T, Chen Q, Lin D-H et al (2011) Self-assembled thienylsilane molecule as interfacial layer for ZnO nanowire/polymer hybrid system. J Photonics Energy 1(1):011107
188. Xu T, Qiao Q (2011) Conjugated polymer-inorganic semiconductor hybrid solar cells. Energy Environ Sci 4(8):2700–2720
189. Xu T, Venkatesan S, Galipeau D et al (2013) Study of polymer/ZnO nanostructure interfaces by kelvin probe force microscopy. Sol Energy Mater Sol Cells 108:246–251

190. Xu T, Yan M, Hoefelmeyer J et al (2011) Exciton migration and charge transfer in chemically linked P3HT-TiO_2 nanorod composite. RSC Adv 2(3):854–862
191. Zhang W, Wang H, Chen B et al (2012) Oleamide as a self-assembled cathode buffer layer for polymer solar cells: the role of the terminal group on the function of the surfactant. J Mater Chem 22(45):24067–24074
192. Li J, Yan M, Xie Y et al (2011) Linker effects on optoelectronic properties of alternate donor–acceptor conjugated polymers. Energy Environ Sci 4:4276–4283
193. Shao S, Zheng K, Pullerits T et al (2012) Enhanced performance of inverted polymer solar cells by using poly(ethylene oxide)-modified ZnO as an electron transport layer. ACS Appl Mater Interfaces 5(2):380–385
194. Yunfei Zhou FSR, Yuan Y, Schleiermacher H-F, Niggemann M, Urban GA, Krüger M (2010) Improved efficiency of hybrid solar cells based on non-ligand-exchanged CdSe quantum dots and poly(3-hexylthiophene). Appl Phys Lett 96(1):013304
195. Yunfei Zhou ME, Veit C, Zimmermann B, Rauscher F, Niyamakom P, Yilmaz S, Dumsch I, Allard S, Scherf U, Krüger M (2011) Efficiency enhancement for bulk-heterojunction hybrid solar cells based on acid treated CdSe quantum dots and low bandgap polymer PCPDTB-T. Sol Energy Mater Sol Cells 95(4):1232–1237
196. Kwong CY, Choy WCH, Djurisic AB et al (2004) Poly(3-hexylthiophene): TiO_2 nanocomposites for solar cell applications. Nanotechnology 15(9):1156–1161
197. Qiao Q, Beck J, James J, McLeskey T (2005) Photovoltaic devices from self-doped polymers. In: Organic photovoltaics VI. SPIE
198. Qiao Q, Su L, Beck J et al (2005) Characteristics of water soluble polythiophene: TiO_2 composite and its application in photovoltaics. J Appl Phys 98(10):094906
199. Qiao Q, Xie Y, McLeskey JJT (2008) Organic/inorganic polymer solar cells using a buffer layer from all-water-solution processing. J Phys Chem C 112(26):9912–9916
200. Yang P, Zhou X, Cao G et al (2010) P3HT:PCBM polymer solar cells with TiO_2 nanotube aggregates in the active layer. J Mater Chem 20(13):2612–2616
201. Liao W-P, Hsu S-C, Lin W-H et al (2012) Hierarchical TiO_2 nanostructured array/P3HT hybrid solar cells with interfacial modification. J Phys Chem C 116(30):15938–15945
202. Hau SK, Yip H-L, Baek NS et al (2008) Air-stable inverted flexible polymer solar cells using zinc oxide nanoparticles as an electron selective layer. Appl Phys Lett 92(25):253301–253303
203. Ka Y, Lee E, Park SY et al (2013) Effects of annealing temperature of aqueous solution-processed ZnO electron-selective layers on inverted polymer solar cells. Org Electron 14(1):100–104
204. Wiranwetchayan O, Liang Z, Zhang Q et al (2011) The role of oxide thin layer in inverted structure polymer solar cells. Mater Sci Appl 2:1697–1701